TOPICAL DELIVERY OF HEPARIN WITH POLYMERIC NANOPARTICLES ON ELECTROSPUN NANOFIBERS

A THESIS SUBMITTED TO
THE GRADUATE SCHOOL OF NATURAL AND APPLIED SCIENCES
OF
MIDDLE EAST TECHNICAL UNIVERSITY

BY

DUYGU DENİZ AKOLPOĞLU

IN PARTIAL FULFILLMENT OF THE REQUIREMENTS
FOR
THE DEGREE OF MASTER OF SCIENCE
IN
BIOTECHNOLOGY

SEPTEMBER 2019

Approval of the thesis:

TOPICAL DELIVERY OF HEPARIN WITH POLYMERIC NANOPARTICLES ON ELECTROSPUN NANOFIBERS

submitted by **DUYGU DENİZ AKOLPOĞLU** in partial fulfillment of the requirements for the degree of **Master of Science in Biotechnology Department, Middle East Technical University** by,

Prof. Dr. Halil Kalıpçılar
Dean, Graduate School of **Natural and Applied Sciences** _____

Assoc. Prof. Dr. Can Özen
Head of Department, **Biotechnology** _____

Prof. Dr. Dilek Keskin
Supervisor, **Engineering Sciences, METU** _____

Prof. Dr. Ufuk Gündüz
Co-Supervisor, **Biological Sciences, METU** _____

Examining Committee Members:

Prof. Dr. Ayşen Tezcaner
Engineering Sciences, METU _____

Prof. Dr. Dilek Keskin
Engineering Sciences, METU _____

Assoc. Prof. Dr. Eda Ayşe Aksoy
Basic Pharmaceutical Sci., Hacettepe Uni. _____

Assist. Prof. Dr. Batur Ercan
Metallurgical and Material Engineering, METU _____

Assist. Prof. Dr. Özge Erdemli
Molecular Biology and Genetics, Baskent Uni. _____

Date: 05.09.2019

I hereby declare that all information in this document has been obtained and presented in accordance with academic rules and ethical conduct. I also declare that, as required by these rules and conduct, I have fully cited and referenced all material and results that are not original to this work.

Name, Surname: Duygu Deniz Akolpoğlu

Signature:

ABSTRACT

TOPICAL DELIVERY OF HEPARIN WITH POLYMERIC NANOPARTICLES ON ELECTROSPUN NANOFIBERS

Akolpoğlu, Duygu Deniz
Master of Science, Biotechnology
Supervisor: Prof. Dr. Dilek Keskin
Co-Supervisor: Prof. Dr. Ufuk Gündüz

September 2019, 89 pages

Skin surrounds underlying organs and preserve the body against harmful microbial, thermal and mechanical effects and skin damages may give rise to crucial disorders or even death. Therefore, skin regeneration is one of the most important issues in tissue engineering. Search on more effective biomaterials that will enhance regeneration while enabling requirements of a healing skin site is an important issue.

In this study, heparin was encapsulated in Poly(lactic-co-glycolic acid) (PLGA) nanoparticles (NPs) and these synthesized NPs were incorporated to Sericin/Gelatin (Ser/Gel) nanofibers which are obtained with the electrospinning method and evaluated for their potency for Skin Tissue Engineering (STE). Sericin and gelatin were chosen as scaffold material to promote the regeneration of skin with these biopolymers and maximize the water retention capacity of the scaffolds which is important for STE. The aim of the use of HP-loaded NP is to provide rapid and effective healing via prolonged and local release of HP in the wound area.

The loading capacity and entrapment efficiency of the nanoparticles were determined as nearly 3% and 60% respectively. Cumulative release of HP from NPs and NP loaded 0/1 and 1/2 Ser/Gel ratio having scaffolds in PBS (pH 7.4, 37°C) was determined as approximately 85%, 60% and 40% over 1-week period, respectively.

Cell viability analysis for scaffolds and heparin loaded PLGA nanoparticles on L929 mouse fibroblast cell line was determined as nearly 80% and higher than 100%, respectively. In the scope of these results, the produced NPs and NP loaded scaffolds were ideal for STE applications.

Keywords: PLGA Nanoparticle, Heparin Delivery, Skin Tissue Engineering, Sericin/Gelatin Electrospinning

ÖZ

HEPARİNİN ELEKTROSPUN NANOFİBERLER İÇİNDEKİ POLİMER NANOPARÇACIKLAR İLE TOPİKAL OLARAK SALIMI

Akolpoğlu, Duygu Deniz
Yüksek Lisans, Biyoteknoloji
Tez Danışmanı: Prof. Dr. Dilek Keskin
Ortak Tez Danışmanı: Prof. Dr. Ufuk Gündüz

Eylül 2019, 89 sayfa

Deri, organları çevreler ve vücudu zararlı mikrobiyal, termal ve mekanik etkilere karşı korur ve cilt hasarları önemli bozukluklara ve hatta ölüme neden olabilir. Bu nedenle cilt yenilenmesi doku mühendisliğinde en önemli konulardan biridir. İyileşen bir cilt bölgesinin gereksinimlerini sağlarken yenilenmeyi artıracak daha etkili biyomalzemeleri araştırmak önemli bir konudur.

Bu çalışmada, heparin, Poli(laktik asit-ko-glikolik asit) nanoparçacıklarına (NP) yüklenmiştir ve bu sentezlenen NP'lar, elektroeğirme yöntemi ile elde edilen Serisin/jelatin (Ser/Gel) nanofiberlerine dahil edilmiş ve Cilt Doku Mühendisliği (STE) çalışmalarındaki potansiyeli için değerlendirilmiştir. Serisin ve jelatin cildin yenilenmesini teşvik etmek ve STE için önemli olan taşıyıcıların su tutma kapasitesini en üst düzeye çıkarmak için biyopolimerler olarak seçilmiştir. HP yüklü NP kullanımının amacı, HP'nin yaralar veya yanıklar tarafından deforme olan bölgede uzun süre ve lokal olarak salımı ile hızlı ve etkili bir iyileşme sağlamaktır. HP, yara iyileşme sürecinde hücreler arasındaki kimyasal sinyalleşmede rol alır.

Nanoparçacıkların yükleme kapasitesi ve enkapsülasyon verimliliği sırasıyla yaklaşık %3 ve %60 olarak belirlenmiştir. HP'nin NP'lardan ve NP yüklü 0/1 ve 1/2 Ser/Gel oranına sahip taşıyıcılardan 1 haftalık sürede PBS (pH 7.4, 37 °C) içerisinde salımı

sırasıyla %85, %60 ve %40 olarak belirlenmiştir. L929 fare fibroblast hücreleri ile PLGA NP'ları ve NP yüklü iskeleleler için hücre canlılığı analizi sırasıyla %100'den fazla ve yaklaşık %80 olarak belirlenmiştir. Bu sonuçlar kapsamında üretilen NP'lar ve NP yüklü iskeleler STE uygulamaları için idealdir.

Anahtar Kelimeler: Nanoparçacık, PLGA, Heparin Salımı, Deri Doku Mühendisliği, Serisin/Jelatin Elektroeğirme

To my precious family

ACKNOWLEDGEMENTS

I would like to thank my supervisor Prof. Dr. Dilek Keskin for her endless support, encouragement and understanding, and also for her valuable advices. I feel so lucky since I worked with my co-advisor Prof. Dr. Ufuk Gündüz. I am grateful to Prof. Dr. Ayşen Tezcaner for her positive attitudes and academic guidance. I would like to thank BIOMATEN since they provided their laboratory facilities for my SEM and FTIR analysis.

I have great appreciation to ES-BIO lab members since we got pleasant and understanding environment in our lab. I have to thank Deniz Atila and Ali Deniz Dalgıç since they gave clues that would broaden my horizon about my thesis all the time. I want to thank Milad Fathi for introducing me nanoparticles, Gerçem Altınordu, Gizem Demir, Gülçin Çiçek, and Sepren Öncü for their friendship. Since we are a very large group, I could not talk about everyone, but I am sure we all have learned from each other. Thank you very much to everyone for their contributions to me.

My dear friends Gizem Damla Yalçın and Özge Atay who supporting me at every moment during my MSc thesis deserve special thanks for their presence. I would like to thank my lovely friends Sonnur Öztürk Noudeh, Canan Işık and Yasin Mısır, who listened to all my troubles, even if they were miles away. I have to thank my engineer friends; Alp Muhiddinoğlu, Berkan Yerlikaya, Koray Yayla and Onur Emre for their helpful presence.

I would like to give my special thanks to my parents, Habibe and Mehmet Beşir Akolpoğlu who are with me every step of my life and to their best gifts for me, my sisters; Fatma Esra Aykoç, Müge Serel Özvatan, and Bahar Cansu Akolpoğlu, due to their endless reliance and support. Last but not least, I am very grateful to my husband, my best friend and my best chance in life Mehmet Başaran for his existence.

TABLE OF CONTENTS

LIST OF TABLES

TABLES

LIST OF FIGURES

FIGURES

LIST OF ABBREVIATIONS

ABBREVIATIONS

A	Absorbance of test wells
CS	Chitosan
DCM	Dichloramethane
DMEM	Dulbecco's Modified Eagle Medium
DMMB	Dimethylmethylene Blue
DMSO	Dimethyl Sulfoxide
ECM	Extracellular matrix
FBS	Fetal Bovine Serum
FGF	Fibroblast growth factor
FT-IR	Fourier Transform Infrared
FT-IR-ATR	Fourier Transform Infrared Spectroscopy-Attenuated Total Reflectance
GAG	Glycosaminoglycans
Gel	Gelatin
GTA	Glutaraldehyde
HP	Heparin
HA	Hyaluronic Acid
L929	Mouse Fibroblastic Cell Line
LMWH	Low Molecular Weight Heparin

MTT	Thiazolyl Blue Tetrazolium Bromide
NP	Nanoparticle
PBS	Phosphate Buffered Saline
PCL	Polycaprolactone
PDGF	Platelet-Derived Growth Factor
PLGA	Poly(Lactic-co-Glycolic Acid)
PMMA	Poly(methyl methacrylate)
PVA	Poly(Vinyl Alcohol)
SEM	Scanning Electron Microscopy
Ser	Sericin
TCP	Tissue Culture Plate
TGF-β	Tansforming Growth Factor-β
Tg	Glass Transition Temperature
VEGF	Vascular Endothelial Growth Factor

CHAPTER 1

INTRODUCTION

1.1. Skin

The biggest organ in the body is the skin and constitutes around 15% of the entire weight of the adult body. It takes role in protection from sunlight, and microbes and also maintaining of homeostasis and thermoregulation in the body. Furthermore, skin prevents loss of water and enables storage of fats, water and vitamin D (Metcalfe and Ferguson, 2007).

Skin tissue is a sensory organ since senses of heat, pressure, pain, and allergens are perceived with it (Walters and Roberts, 2002).

Skin form from 3 layers (Figure 1.1);

- The first layer is the epidermis (stratum baseline). It is water-impermeable and gives color to the skin. Keratinocytes and melanocytes are in this part. Epidermis thickness is approximately 75–150 μm (Goldsmith, 1991). The nonviable epidermis, which is the outermost layer in skin, is called stratum corneum.
- Beneath the epidermis, the layer containing connective tissue is found and it is named as the dermis. It contains, hair follicles, glycosaminoglycans (GAGs), nerve endings glands and blood vessels. The dermis mostly consists of extracellular matrix (ECM) formed by interwoven collagen fibrils. Most of the ECM is generated and preserved by fibroblast cells that are the major cell type of dermis.
- The dermis and the epidermis together are also referred to as cutis, which has a thickness of 1.5–2.5 mm (Laurent et al., 2007).

- The subcutaneous fat under the dermis is named as hypodermis. With the help of fat it absorbs shock an isolate the tissue (Hoffman M., 2014). It is mainly composed of adipose cells and the thickness of this layer differs according to the site of the body.

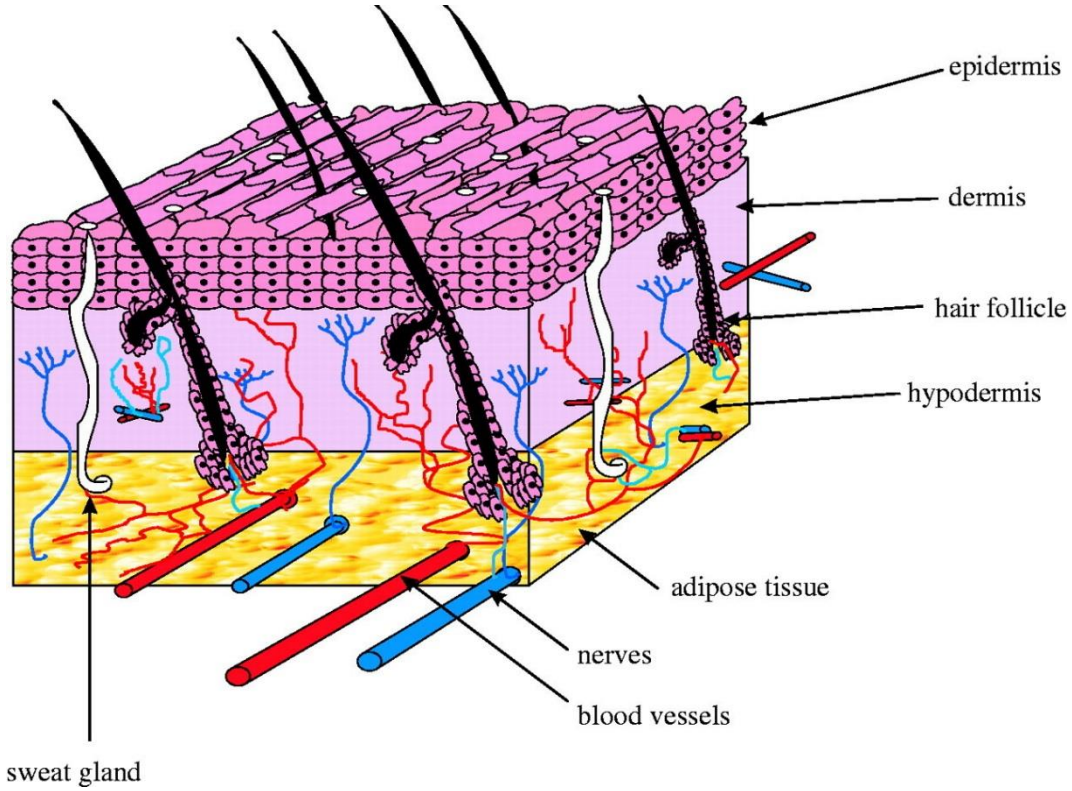

Figure 1.1. A schematic of skin structure (Metcalfe & Ferguson, 2007)

1.1.1. Wounds

Wounds can be described as internal or external damage or brake occurring in the skin due to physical, thermal or medical impacts (Gonzalez et al., 2016). Classifications of wounds are based on number of affected skin layers or on affected skin area. Defects affecting the epidermis is called as a superficial wound. However, if injury influences skin through epidermis and dermal layers, it is referred as partial-thickness wound.

Wounds penetrating to subcutaneous fat tissue and deeper layers, in addition to epidermis and dermis, is named as full-thickness wounds (Boateng et al., 2008).

Burns are one type of wound that involve injuries occurring on the skin because of exposure to heat, sun, or other forms radiation, chemicals, and electricity (American Society for Surgery of the Hand, 2014). According to severity of the burns, they are classified as below;

- *1st-degree burns* occur in the epidermis and result in pain and reddening of the epidermis
- *2nd degree burns* damage both epidermis and dermis layers. Generally, blisters develop with second-degree burns.
- *3rd-degree burns* affect hypodermis layer of skin and cause burning of hair follicles, sweat glands, muscles, and bones as well.

1.1.2. Wound Repair

Skin takes role as a protective barrier in the body. Loss of large part of a skin because of the wounds or burns may give rise to crucial disorder or even death. Therefore, skin repair is one of the most important issues in tissue engineering.

Wound healing is a complex series of events, including collaboration of several cells to reestablish cellular homeostasis. This dynamic biochemical pathway is composed of four overlapping but well-defined phases: hemostasis, inflammation, proliferation, and remodeling (Figure 1.2).

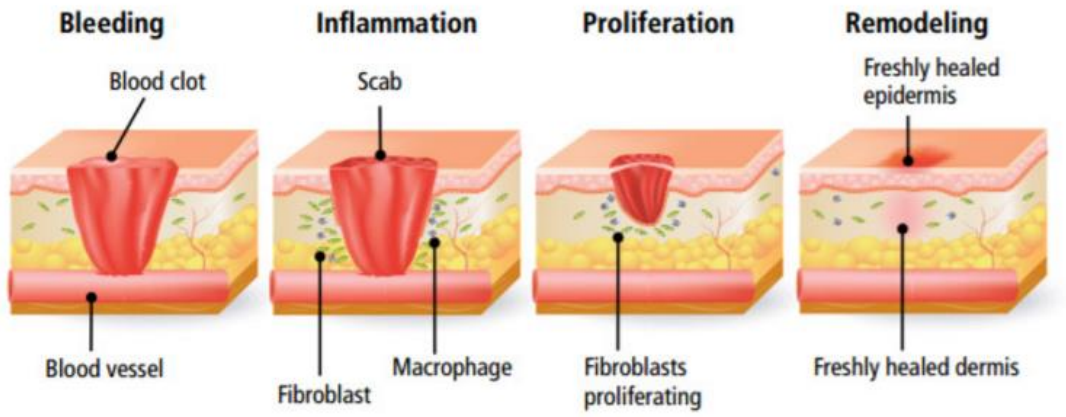

Figure 1.2. Sequential scheme of the stages in tissue repair (Maynard J., 2015)

1.1.2.1. Hemostasis Phase

As soon as the injury occurs, coagulation step begins. The purpose of this step is not only to prevent excess bleeding but also to gain a matrix for cells that will be required in other healing processes.

Coagulation mechanism is triggered by extrinsic and intrinsic pathways to restrict blood loss. When blood reaches the wound site, its components and platelets encounter extracellular matrix components like collagen and this event results in clotting factor secretion from the platelets. Blood clot that is composed of fibrin, fibronectin, and thromboplastin, forms.

In the platelet cytoplasm, α-granules having platelet-derived growth factor (PDGF), transforming growth factor-β (TGF-β) epidermal growth factor and insulin-like growth factors are present. These growth factors and cytokines take role in wound repair by recruiting neutrophils and macrophages, endothelial cells and fibroblasts to the wound site. Attraction of leukocytes to the wound site gives rise to starting of inflammatory phase (Velnar, Bailey, and Smrkolj, 2009).

1.1.2.2. Inflammatory Phase

The second stage for wound repair is inflammation. At the inflammation phase, the wound is protected from both excessive bleeding and infections. Neutrophils take role

in phagocytosis to get rid of microorganisms, impurities and destroyed tissue. Macrophages are drawn to the wound site by cytokines such as TGF-β, leukotriene B4 and platelet factor IV, clotting factors, products of collagen and elastin decay. Inflammatory response acts as a reservoir of tissue growth factors, especially TGF-α, heparin-binding epidermal growth factor, and fibroblast growth factor (FGF) so that activates keratinocytes, fibroblasts, and endothelium cells. These leukocytes, growth factors, and cytokines cause swelling, heat, pain, and redness that occur during wound healing (Velnar et al., 2009).

1.1.2.3. Proliferative Phase

Proliferative phase occurs when the wound begins to heal, and new tissue forms to rebuild the wound site (Singh, Young, & McNaught, 2017). It starts commonly on the third day of injury and lasts for about two weeks. Several steps that can take place in this phase are indicated below;

- Fibroblast migration is induced to the wound site by factors such as TGF-β and PDGF
- Collagens that takes role in the intracellular matrix formation are synthesized.
- Angiogenesis that is new blood vessel formation triggered by FGF, vascular endothelial growth factor (VEGF), PDGF, angiogenin, TGF-α and TGF-β

1.1.2.4. Remodeling Phase

New epithelial tissue formation occurs in this phase. Most of the cells effective in the wound healing undergo apoptosis such as endothelial cells, macrophages, and myofibroblasts. Few cells, collagen and other extracellular matrix proteins remain in the wound area. Remodeling of collagen from type III to type I occurs which strengthens the repaired tissue (Reinke & Sorg, 2012). At the end, scar tissue formation is seen with a decreased number of cells and blood vessels in the wound site.

1.2. Controlled Drug Delivery

Drug delivery is the method used for administration of pharmaceuticals in the needed region of the body for therapeutic purposes within or as attached to a suitable carrier molecule or structure.

Nanoparticles which are used as nanocarriers for drug delivery purposes can be classified basically as liposomes, solid lipid nanoparticles, and polymer nanoparticles (Saghazadeh et al., 2018).

Liposomes are spherical lipid bilayers which are consisting of phospholipids and steroids.

With surfactant-stabilized lipids, solid lipid nanoparticles are synthesized. These molecules are solid both at room and body temperatures. Its high physical stability and biocompatibility make it preferable drug carrier.

Polymer-based nanoparticles can be used as carriers in the pharmaceutical field because controlled release can be achieved with such drug delivery systems. Biocompatible and biodegradable polymers are preferred for nanoparticle production (Krishnaswamy & Orsat, 2017). Nanoparticles offer a potential strategy for targeted delivery of therapeutic drugs by prolonging their half-life through sustained release. Biodegradable polymer-based nanoparticles can be used to deliver the therapeutic agent to target region, to reduce the systemic side effects of a drug, to increase the biocompatibility of the carried agent and to increase bioavailability of the drug (Tiwari et al., 2012).

1.2.1. Polymer-Based Drug Delivery Systems

Polymer nanoparticles can be classified as nanospheres and nanocapsules (Viswanathan, Muralidaran, & Ragavan, 2017). While nanospheres are composed of homogeneously distributed structure in the whole nanoparticle, nanocapsules show core-shell structure and drug is mostly encapsulated within a polymer shell.

Examples for synthetic polymers that are used for nanoparticle production are poly-e-caprolactone, polyacrylamide and polyacrylate, Poly(lactide-co-glycolide) (PLGA) and Poly(lactide) (PLA). Examples for natural polymers are; albumin, chitosan, and gelatin (Rangari, 2015). Degradation behavior of polymers in the body can be differentiated as; biodegradable and non-biodegradable. Biodegradable polymers are hydrolyzed in the body and degraded to its monomers, e.g., PLGA degradation leads to lactic acid and glycolic acid formation.

Critical parameters, such as loading of the drug into the spheres and release profiles, which affect the properties of nanoparticles, may depend on the characteristics of the polymer.

1.2.1.1. PLGA

PLGA is a synthetic polymer commonly used in biomedical applications owing to its biocompatibility, biodegradability and mechanical strength (Zakharova et al., 2017). PLGA is approved by the Food and Drug Administration (FDA, USA) for drug delivery due to low systemic toxicity of PLGA and its degradation products compared to other polymers. When PLGA is degraded, lactic acid and glycolic acid are formed (Figure 1.3). These products are metabolized by participating in the Kreb's Cycle. Thus, they are eliminated from the body as carbon dioxide and water as a result of biochemical activities in the cell (Muthu, 2010).

Different copolymer ratios of PLGA are named based on the ratio of lactic acid to glycolic acid. As an example, PLGA 85:15 indicates that the copolymer is composed of 85% lactic acid and 15% glycolic acid (Gentile et al., 2014).

In the lactic acid part of PLGA copolymer, methyl side groups are present, and this makes it more hydrophobic than glycolic part. Therefore, PLGA copolymers having high lactide ratio are more hydrophobic, and therefore, degrade more slowly in the body. Since PLGA can be hydrolyzed in the body, some parameters of a copolymer can change with time, such as the glass transition temperature (Tg), moisture content and molecular weight (Makadia & Siegel, 2011).

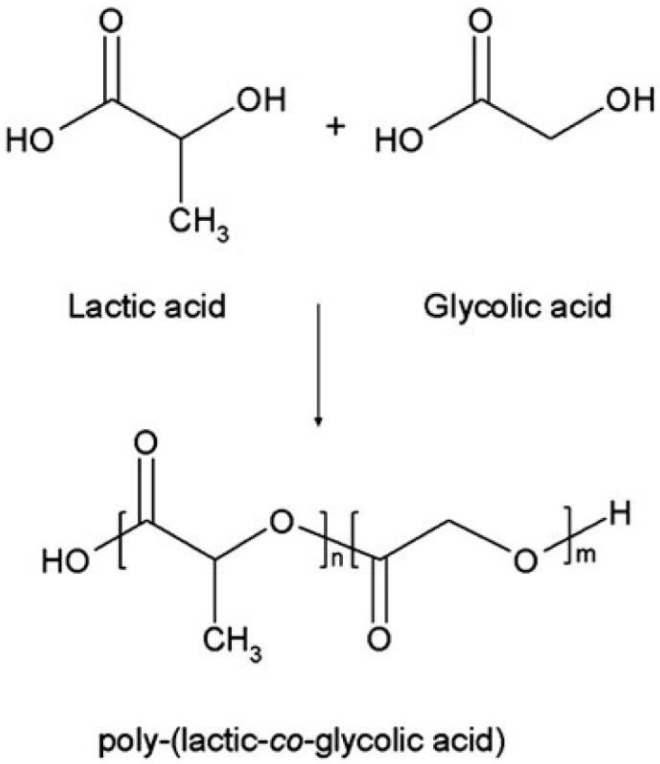

Figure 1.3. PLGA and its monomers chemical structures (Gentile et al., 2014)

There are several fabrication techniques for PLGA nanoparticle synthesis. They are namely single emulsion solvent evaporation method, double emulsion solvent evaporation method and spray drying method.

For water-soluble drug encapsulation, the most feasible method is water-in-oil-in-water (w/o/w) emulsion method. In this method, aqueous solution of the drug is prepared and then it is added to organic phase consisting of polymer solution as the solvent (such as dichloromethane (DCM) or chloroform) by vigorous stirring to get water-in-oil emulsion. Next, the water-in-oil primary emulsion is added to aqueous solution of a surfactant to obtain second emulsion emulsified. The organic solvent is then allowed to evaporate. Encapsulation efficiency and particle size depend on the used solvents and rate of stirring (Iqbal et al., 2015).

1.2.2. Bioactive Agents Used in Skin Regeneration

Bioactive agents which are used in skin regeneration are the natural products take role in one or more wound healing phases by improving epithelial cells proliferation, ECM formation and recruitment of cytokines, growth factors various inflammatory mediators to wound area (Tsala, Amadou, & Habtemariam, 2013).

Example for bioactive agents can be used in wound healing purposes; antibiotics, growth factors, natural compounds and oxide nanoparticles (Dash & Hsia, 2019) Also, heparin can be thought as a bioactive agents for skin regeneration since they have significant biological activity as co-receptors for a variety of growth factors, cytokines, and chemokines in wound healing processes (Khurshid & Pye, 2018).

1.2.2.1. Heparin

Heparin is a molecule having the highest known negative charge density among biological molecules. It is a highly sulfated glycosaminoglycan (sGAG) and has been widely used as a anticoagulant (Saliba, 2001) (Figure 1.4). GAGs take role in signaling in the wound healing process by stimulating cell differentiation, migration, proliferation and arrangement, and maintenance of extracellular matrix formation. GAGs boost these features by binding and regulating several cytokines, growth factors, and chemokines such as heparin-binding growth factors, proteolytic enzymes, and protease inhibitors (Olczyk, Mencner, & Komosinska-Vassev, 2015). Heparin relieves pain, prevents clotting and inflammation, improves blood flow and accelerates healing. In nature, heparin produced in the body of mammals by basophils and mast cells and it can be found in various sizes (Rosenberg & Lam, 2006).

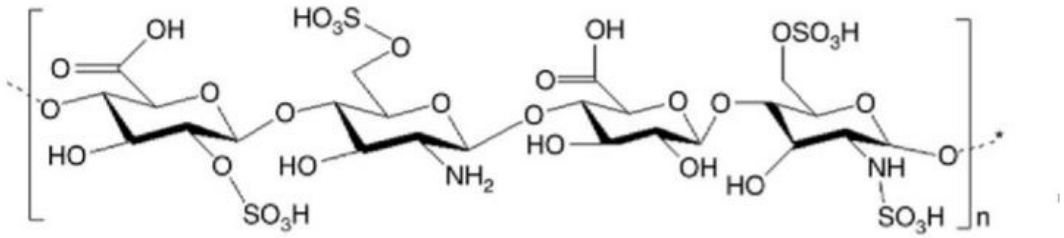

Figure 1.4. Chemical structure of heparin ((Nurunnabi et al., 2017)

Due to the specific physicochemical properties of heparin, it is the most suitable treatment for the patient with parenteral routes, but due to the low half-life, it is eliminated in a short time. For this reason, free heparin drugs should be administered in every two hours in the hospital, and this is not a practical solution according to current technology (Radivojša, Grabnar, & Grabnar, 2013). The low half-life and frequent application to the patient also cause systemic side effects.

Topical application of heparin has great importance in terms of decreasing the systemic side effects and increasing the compliance of the drug to the patient. The properties of heparin that is topically administered to the patient are lined up below (Song & Kim, 2006);

• has anti-inflammatory feature,

• pain killer and protect cells,

• promotes neoangiogenesis,

• reverses stasis (deceleration of blood flow),

• promotes epithelialization,

• provides collagen restoration,

• has anticoagulant properties,

• improves the quality of the skin.

Mediation of *in vitro* impacts of growth factors that take role in tissue repair can be done by heparin. That is; heparin has beneficial effects on basic fibroblast growth factor (bFGF), vascular endothelial growth factor 1 mediation and fibroblast proliferation and growth factor-beta 1 (TGF- β1) (Lin, Fabbi, & Driver, 2011)

In the study that is published by Liu et al., heparin containing hydrogels showed recruitment of bFGF to the wound site (Liu et al., 2007). In another *in vitro* study, expression of bFGF and TGF-β1 are induced by heparin on human fibroblasts (Carroll & Koch, 2003).

Since heparin takes role in the proliferation of several cell types, it helps wound healing. Owing to advances in nanotechnology, nanoparticles offer a potential strategy for targeted delivery of heparin on wound or burn site and with this application prolonging of half-life of heparin is possible through sustained release.

1.3. Wound Dressings

Previously, gauze has been used to cover wounds as then, dressings have been considered only to create a moist environment, and to supply best conditions for wound healing. However, gauze dries with time and can cause tissue damage when it is removed. On the other hand, wound dressings are preferred to protect the wound site from microorganisms and sunlight as well as supporting homeostasis in the body, maintain moist environment and gaseous exchange of skin. These properties of occlusive dressing to contribute increase in cell proliferation and retaining wound site in optimal condition (Jones, Grey, & Harding, 2006). Moreover, in recent years, wound dressing materials are designed to deliver drugs, growth factors or cells directly to the region of wound (Ovington, 2007).

The dressing is intended to be in contact with the wounds. When the wound is enclosed with dressing, proteinases, supplement, and growth factors are persistently presented to wound sites. Wound dressing assists in more rapid re-epithelialization, collagen production, increase in angiogenesis by creating hypoxia at the injury bed. Wound bed

pH goes down so that decline in the contamination of injured site can occur (Dhivya, Padma, & Santhini, 2015).

1.3.1. Important Features for Wound Dressings

Wound dressing choice should be made regarding to its properties. Some of the properties, that ideal wound dressing should have, are listed below;

- Having an ability to maintain moist environment at the wound site (Sarabahi, 2012)
- Capable to keep body temperature at the desired range to enhance blood flow in the wound area (Sood, Granick, & Tomaselli, 2014)
- Improving epidermal cells migration to the wound bed (Jones et al., 2006)
- Supporting angiogenesis and promoting connective tissue (Dhivya et al., 2015)
- Being sterile, non-toxic and non-allergenic (Dhivya et al., 2015)
- Being removed easily after healing and should not adhere to wound (Dhivya et al., 2015)
- Providing gaseous exchange between wound and atmosphere (Dhivya et al., 2015)
- Having antibacterial property (Dhivya et al., 2015)
- Protecting the injury site from further trauma (Dhivya et al., 2015)

1.3.2. Types of Wound Dressing

It is important to select appropriate wound dressing type according to the features of the wound, such as depth and cause of damage, bacterial profile of surrounding and stage of wound repair (Dhivya et al., 2015). Various wound dressing types are given in Table 1.1.

Table 1.1. Types of the wound dressing (Zahedi et al., 2010)

Wound dressing type	**Properties**	**Example**
Traditional wound dressing	• Made up of cotton, rayon or polyesters • Protect the wound site from bacterial infections • Require frequent changing • Adhere to the wound and damage wound bed	gauze, lint, plasters, bandages
Interactive wound dressing	• Restrict dehydration and promote healing • Act as a barrier to resist bacterial penetration into the wound environment	Semi-permeable films, amorphous hydrogels
Regenerative wound dressing	• Promote cell attachment and cell proliferation (Zhou et al., 2008) • Have biocompatibility, highly biodegradability nature • Fill the wound site (Dabiri, Damstetter, & Phillips, 2016) • Composed of active ingredients, such as antimicrobials and antibiotics	collagen, HA, CS, alginate, and elastin

1.4. Electrospinning

Electrospinning is a widely used method for fiber fabrication because it is a practical, robust and cheap technique that allows producing thin fibrous structures from several polymers and composite materials (Bhardwaj & Kundu, 2010). With electrospinning, it is achievable to have fibers with high surface-to-volume ratio and this makes it a suitable choice for 3D engineered-structures. Electrospun fibers have diverse application areas, such as drug delivery, tissue engineering, biosensors, medical textiles, cosmetics, enzyme immobilization and wound dressings (Agrahari, Agrahari, Meng, & Mitra, 2017).

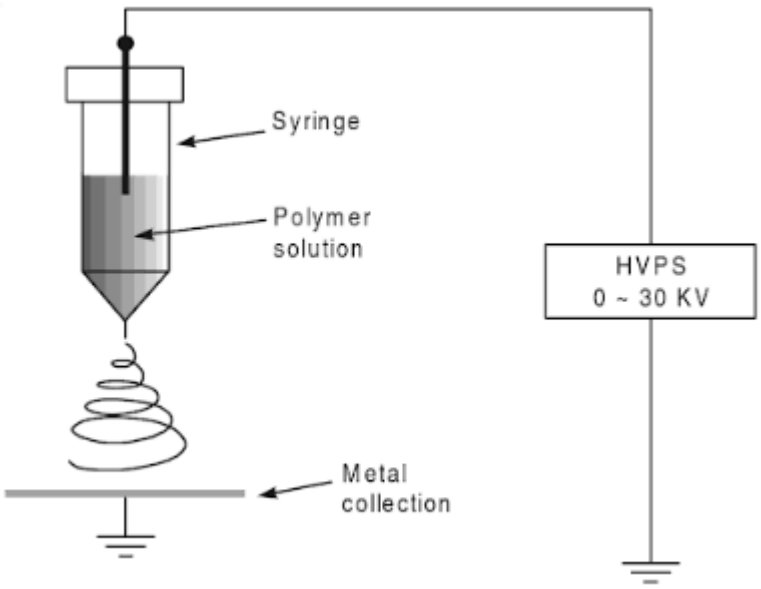

Figure 1.5. Schematic illustration of electrospinning set-up (Panda H., 2009)

Electrospinning is the application of electrostatic forces on a dissolved polymer solution to generate stable polymer fibers.

During electrospinning, a polymer solution in syringe is connected to high voltage power supply and a syringe pump directs the polymer solution to spinneret (Figure 1.5). The basics behind this process are that formed electric charges in polymer solution produces a force that resists the surface tension, and this results in movement

of polymer solution in the direction of electrical field (Adnan, Sajjad & Kanga, 2015). Therefore, fibrous structure forms on a grounded collector while the solvent evaporates (Bognitzki et al., 2001).

Even though electrospinning is a relatively simple method compared to other scaffold construction methods, parameters related to experimental set-up and conditions should be tailored to get fibers in a desired size and morphology (Sill & Recum, 2008).

1.4.1. Parameters Affecting Electrospinning Processing

Several parameters affect the morphology and characteristics of produced fibers. Smooth and bead-free fibers can be obtained by optimization of the parameters. Factors affecting electrospinning can be separated into three as; electrospinning set up variables, polymer solution properties, and environmental conditions.

1.4.1.1. Electrospinning Set-up Variables

Spinning voltage, flow rate and distance between tip and collector are among the important parameters that need to be optimized. For example, when the applied voltage is increased, fiber diameter decreases up to a critical point. At too high voltages bead formation can occur. At lower flow rates generally formed fibers are bead-free and with smaller diameters (Deitzel et al., 2001).

The other important variable affecting nanofiber morphology is a distance between tip and collector because distance influences deposition of polymer on the collector, evaporation of solvent and bead formation in fibers (Haider, Haider, & Kang, 2018).

1.4.1.2. Polymer Solution Properties

Polymer solution properties are affected mostly from the solvent choice. Dielectric constant, density and boiling point of solvent are significant parameters to prepare fine electrospun fibers. High density and volatility of the solvent lead to decrease in fiber diameters (Wannatong, Sirivat, & Supaphol, 2004). The boiling point of the solvent is the determinant of volatility. Volatile solvents are generally preferred for rapid

dehydration of the solution before reaching to the collector, however, highly volatile solvents can result in plugging at the tip of the syringe and block the process.

Solution viscosity is directly proportional to polymer solution concentration and molecular weight of polymer (B. S. Gupta & Moghe, 2013). Hence, when concentration of the polymer solution (thus viscosity) increases, chain entanglements in polymer solutions occur and it becomes easier to cope with the surface tension. Viscosity/concentration increase results in beadless and uniform electrospun nanofibers up to specific value. In general, polymers having higher molecular weight form less number of beads on fibers since large number of entanglements of polymer chains occur in solution (Wei, Tao, & Xu, 2012).

The effect of electrical conductivity on the fiber characteristics generally noted as an increase in the conductivity of the solution leads to a significant reduction in the diameter of the nanofiber. The reason for this situation is that when voltage is applied a solution having high electrical conductivity is exposed to a high tensile force and as a result decrease in fiber diameter occurs (Pillay et al., 2013).

1.4.1.3. Environmental parameters

Environmental conditions such as temperature, relative moisture, and vapor pressure also influence fabrication of fibers and fiber properties (Megelski et al., 2002).

High ambient temperature causes decreas in both viscosity and surface tension but increases solvent evaporation and these parameters work oppositely. However, studies showed that rise in temperature leads to decrease in the mean fiber diameter if there is balance between these parameters (De Vrieze et al. 2009, Yang et al. 2017).

Effect of relative humidity on diameter size of nanofiber depends on characteristics of the used polymer. However, relative humidity increase can result in the formation of pore on the fabricated fibers (Megelski et al., 2002).

1.4.2. Sericin

Silk is composed of fibroin and sericin proteins. Sericin is a biopolymer found in the cocoon of the silkworm, *Bombyx mori*. Sericin can be used as a glue and it connects fibroins to each other. Sericin contains mostly serine, aspartic acid, glycine and threonine in its structure as amino acid so that it is water-soluble. Amino acid composition in sericin protein is shown in Table 1.2 (Wang & Zhag, 2011).

Table 1.2. Amino acid composition of sericin (Wang and Zhag 2011)

	Amino Acid	**Mol % of amino acids found in sericin**
Nonpolar hydrophobic	Alanine	6.70
	Valine	4.05
	Leucine	1.49
	Isoleucine	1.02
	Phenylalanine	0.67
	Methionine	0.31
	Proline	0.81
Polar uncharged	Glycine	17.85
	Serine	25.50
	Threonine	7.47
	Tyrosine	3.10
	Cysteine	0.38
Polar acidic	Aspartic acid	18.38
	Glutamic acid	5.74
Polar basic	Lysine	2.08
	Arginine	3.12
	Histidine	1.32

Several properties of sericin are indicated in Table 1.3.

Table 1.3. Properties of sericin (Ersel et al. 2016)

Properties of Sericin
○ UV resistance ○ antioxidation ○ moisture absorbance ○ biocompatibility ○ proliferation-promoting effects ○ natural cell adhesive property ○ low immunogenicity

Sericin protein feature in wound healing through four mechanisms (Qi et al., 2018);

- prevents infection while wound healing;
- stimulates VEGF and EGF expression and accordingly promote angiogenesis
- regulates TGF-β1 and TGF-β3 expression so reduce scar formation
- enhances stem cell migration to injury sites and also helps regeneration of new tissue

Sericin is a very attractive protein to use in broad variety of applications because of its preferable properties. It is widely preferred in various research areas such as drug delivery, pharmaceuticals, food engineering, tissue engineering, and regenerative medicine (Ahsan et al., 2018). Because of its capability to stimulate skin regeneration and dermal wound healing, it is one of the most effective candidate polymers for wound dressing applications. Furthermore, these feasible properties of sericin can be enhanced by blending it with other polymers (Kundu et al., 2008). Several examples for sericin containing wound dressing studies are summarized in Table 1.5.

1.4.3. Gelatin

Gelatin (GE) is a protein obtained by hydrolysis of native collagen that is found in the skin, bone, and cartilage tissues. GE is less immunogenic compared to collagen. It has cationic, anionic, and hydrophilic functional groups (Zhu & Marchant, 2011). The protein content of porcine skin gelatin is shown in Table 1.4 (Nhari et al., 2011). Because of its biodegradability, biocompatibility and low cost, GE is mainly preferred in the pharmaceutical and biomedical applications.

Two main functional properties of gelatin are; its gelling and surface properties. Gelation of gelatin is about the reverse of coil-to-helix conformation change. When temperature of solution drops below 30 °C, helices form, equilibrium is lost, therefore, gelatin gels can melt at high temperatures (Balusamy, Senthamizhan, & Uyar, 2017).

Crosslinking of GE affects material mechanical and physical properties such as; thermal properties and swelling characteristics. Commonly, GE is known for its ability to form film. Nevertheless, it does not seem capable to form fibers with conventional spinning methods. Fine, nanosized fibers can be achieved with electrospinning method (Zhang et al., 2006).

Table 1.4. Porcine skin gelatin amino acid composition (Raja Nhari et al., 2011)

	Amino Acid	**The number of amino acid residue found in per 1000 residue**
Nonpolar hydrophobic	Alanine	80
	Valine	26
	Leucine	29
	Isoleucine	12
	Phenylalanine	27
	Methionine	10
	Proline	151
Polar uncharged	Glycine	239
	Serine	35
	Threonine	26
	Tyrosine	7
Polar acidic	Aspartic acid	41
	Glutamic acid	83
Polar basic	Lysine	27
	Arginine	111
	Histidine	Not detected

1.5. Electrospun Nanofibers as a Wound Dressing

Nanofibrous dressings are widely preferred due to similarity to the natural extracellular matrix (ECM). High porosity and high surface area-to-volume ratio of electrospun nanofibers make them a suitable material for wound healing applications (S. Chen et al., 2017). Porosity is important since smaller pore sizes can restrict

bacterial invasions. The high surface-area-to-volume ratio of fabricated material enables cell attachment, enhances epithelial cells proliferation and differentiation (Zafar et al., 2016).

Furthermore, it is possible to construct nanofibers from the combination of different synthetic and natural polymers with a simple and facile way with electrospinning compared to phase separation or self-assembly techniques which are other fabrication methods commonly used for polymer materials (Haider et al., 2018).

Usage of natural polymers increases interaction of the constructed material with biomolecules involved in the healing process. The studies, including sericin and gelatin natural polymers, are summarized in Table 1.5.

Table 1.5. Wound dressing systems composed of natural polymers

Materials	**Structure**	**Properties**	**References**
Sericin/Chitosan	Film	protection from ultraviolet light	(Pankaew, White, & Naemchanthara, 2015)
PVA/Chitosan/ Sericin	Nanofibrous Matrices	cytocompatible and hemocompatible, minimize infection and inflammation	(Sapru et al., 2018)
Silk Sericin	Gel	antioxidant properties and enhance the thickness of epidermis and increase vascularization in wound area	(Ersel et al., 2016)
PVA/ Sericin	Nanofibrous Matrices	increased antioxidative effect and improve fibroblast cells proliferation	(Ersel et al., 2016)
Sericin/Collagen	Nanofibrous Matrices	enhanced oxygen permeability, cellular attachment, and antibacterial properties	(Akturk et al., 2011)
Cellulose/Gelatin	Hydrogel	improved oxygen permeability by macro- and micro-porous structure	(Pei et al., 2015)
Sericin/Gelatin	Film	improved cell attachment and cell viability reduced immunogenicity	(Mandal, Priya, & Kundu, 2009)
Gelatin/Collagen Type I/Chondroitin 6-Sulfate	Dermis Powder/Gelatin Paste	the proliferation of fibroblasts and improvement of blood vessel formation	(Jang et al. , 2018)
Chitosan-Gelatin	Sponge	rapid wound healing and antibacterial properties	(Deng et al., 2007)

1.6. Aim of the Study

In this study, it is aimed to construct scaffolds composed of sericin and gelatin polymers in the form of electrospun fibers carrying heparin-loaded nanoparticles via wet electrospinning technique for skin tissue engineering applications. Heparin (HP) is encapsulated in Poly(Lactic-co-Glycolic Acid) (PLGA) nanoparticles (NPs) and these synthesized NPs were incorporated to electrospun sericin/gelatin composite nanofibers for better management serious skin injury/illnesses (Figure 1.6).

The purpose of the study was to develop a new wound dressing that can enable rapid and effective healing in the region that has deformed by wounds or burns. While recruiting of growth factors and cytokines to wound area with the help of heparin, promoting the regeneration of skin with natural polymers (gelatin and sericin) at the wound site is expected. In this study, electrospun fibers were obtained for the first time with sericin and gelatin. Also, decreasing side effects of heparin on healthy tissues and systemic circulation with the controlled local release was aimed. Crosslinking of sericin/gelatin composite material was performed to augment mechanical strength and to enhance durability of the developed wound dressing through healing period.

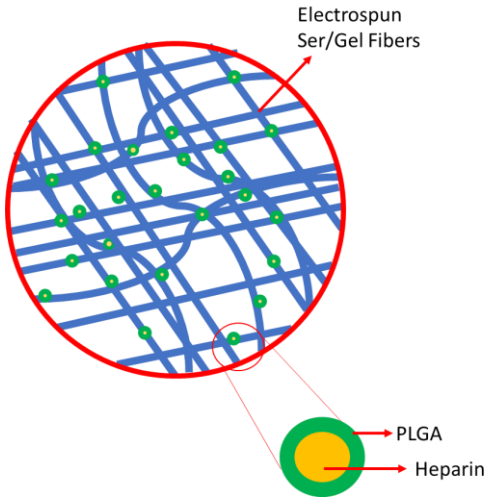

Figure 1.6. Schematic representation of Ser/Gel nanofibers containing HP-loaded NPs.

CHAPTER 2

MATERIALS AND METHODS

2.1. Materials

For empty and heparin loaded PLGA nanoparticle synthesis: PLGA (75:25), MW:7-14 kDa was bought from Boehringer Ingelheim (Germany). Hot water soluble Poly(vinyl alcohol) (PVA) was purchased from Sigma-Aldrich (USA). Heparin sodium salt from porcine intestinal mucosa (Grade I-A, ≥180 USP units/mg) was purchased from Sigma-Aldrich (USA). Dichloromethane (DCM) was the product of Merck (Germany)

For Electrospun scaffolds: Dry sericin was obtained from Kirman İplik Limited Company (Bursa, Turkey). Type A gelatin, from porcine skin was bought from Sigma (Germany).

For *in vitro* cell culture analysis: Dulbecco's Modified Eagle's Medium (DMEM) high glucose (4.5 g/L) with L-glutamine, heat inactivated fetal bovine serum (FBS), trypsin EDTA and penicillin/streptomycin were purchased from Biochrom (Germany). Dimethyl sulfoxide (DMSO) was supplied by AppliChem GmbH (Germany). Thiazolyl blue tetrazolium bromide (MTT bromide, approx. 98 % TLC) and trypan blue solution (0.4%) were purchased from Sigma-Aldrich Chemie GmbH, Germany. Alamar Blue cell viability reagent was bought from Invitrogen by Thermo Fisher Scientific (Oregon, USA).

For Heparin detection and release experiments: Dimethyl methylene blue (DMMB) was obtained from Aldrich (Germany). Glycine electrophoresis purity reagent was purchased from Bio-rad (Hercules, CA). Sodium chloride and glacial acetic acid used

for DMMB assay were bought from Merck. Cell culture inserts for 24-well plates was bought from Thermo Fisher (USA).

2.2. Methods

2.2.1. Preparation of Heparin-Loaded Polymer Nanoparticles

In this study, double emulsion (w/o/w) and solvent evaporation method was used to prepare polymeric NPs (Iqbal et al., 2015) (Figure 2.1). The prepared 4500 IU/mL aquous solution of Heparin sodium was added to 2 mL 5% PLGA solution in DCM and sonicated for 60 sec. to form the first emulsion; water/oil (w/o) phase by ultrasonicator with 20% amplitude. After adding 10 mL aqueous PVA solution (3% w/v) to this mixture, solution was sonicated for 90 sec to obtain 2nd emulsion (water/oil/water, w/o/w). The resulting emulsion was diluted with PVA solution (0.3% w/v) and allowed to evaporate the organic solvent for 4-5 hours under mechanical stirring with a rotation speed of 1000 rpm. After removal of the organic solvent, the NPs were washed three times with distilled water and collected by centrifugation (10000g, 20 min.). They were then freeze dried with Labconco Freeze Dryer (Kansas, USA) and stored at desiccator at 4 °C until use.

For the synthesis of empty PLGA NPs, same were followed, except administration of heparin sodium salt to PLGA solution in DCM.

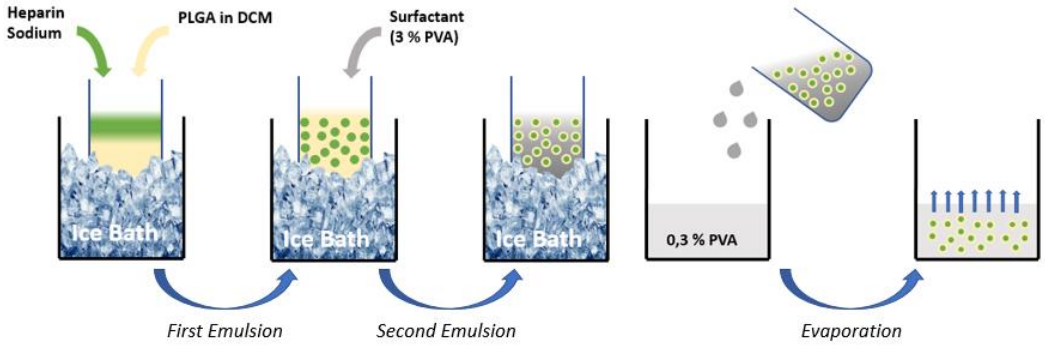

Figure 2.1. Synthesis of PLGA nanoparticles with double emulsion solvent evaporation method

2.2.2. Determination of Heparin Loading and Encapsulation Efficiencies of Nanoparticles and Investigation of Heparin Release Profiles

NPs were centrifuged for 20 min. at room temperature immediately after solvent evaporation. The amount of drug that was loaded into nanoparticles was determined indirectly by measuring the amount of free HP present in the collected aqueous phase after centrifugation of the drug loaded nanoparticles.

Calibration curve with Dimethylmethylene Blue (DMMB) was conducted to calculate the concentration of the unentrapped heparin. Working principle of the 1,9-dimethylmethylene dye is based on formation of changes in dye color when dimer of the dye and sulfated GAGs' polyanion formed ionic interaction (Templeton, 1988). DMMB Assay was done with the protocol performed by Thomas and Gesteira (Coulson-Thomas & Gesteira, 2016). 20 µl heparin sodium solution having different concentrations were mixed with 200 µl DMMB dye solution in 96 well plate. Absorbance measurements was done at 525 nm by using SpectraMax iD3 Multi-Mode Microplate Reader from Molecular Devices LLC (California, USA).

Heparin encapsulation efficiency was calculated to determine the percentage of heparin entrapped in the polymeric NPs with respect to theoretical value. Loading capacity of the NPs was determined to show the amount of heparin (IU or mg) loaded per g of polymer. Determination of percent entrapment efficiency (EE%) and loading capacity (LC) were performed by using formulas below;

$$\text{EE \%} = \frac{Weight\ of\ drug\ added - Weight\ of\ unentrapped\ drug}{Weight\ of\ drug\ added} * 100$$

$$\text{LC} = \frac{Weight\ of\ drug\ added - Weight\ of\ unentrapped\ drug}{Weight\ of\ drug\ added + Weight\ of\ polymer}$$

In vitro release analysis was performed by the dialysis method. 5 mg heparin loaded nanoparticles were placed into a dialysis membrane with 14,000 molecular weight cut off. Dialysis was done against 4 mL phosphate-buffered saline (PBS, pH 7.4, 0.1 M) solution by stirring it at 37°C in a water bath. Release samples were taken at 1, 2, 6,

12 and 24 hours for the first day and the samples were taken at second, third and seventh days. The amount of released heparin was determined using the standard curve of heparin in PBS (pH 7.4, 0.1 M) by using DMMB assay.

2.2.3. Investigation of Physicochemical Properties of Heparin Loaded Nanoparticles

Severel methods were used for the characterization of synthesized nanoparticles.

2.2.3.1. Fourier Transform Infrared (FTIR) Spectrometer Measurements

Chemical properties of nanoparticles were determined by Fourier Transform Infrared (FTIR) spectrometer (Bruker IFS 66/S FTIR) in Center of Excellence in Biomaterials and Tissue Engineering (BIOMATEN) at METU (Ankara, Turkey). It was performed by mixing nanoparticle powder with a ratio of 10% (w/w) with KBr powder and followed by crashing in a mortar. Then discs of the mixture were prepared and analyzed. The analysis was performed in wavenumber range 400- 4000 cm^{-1}, with a resolution of 4 cm^{-1}.

2.2.3.2. Scanning Electron Microscopy Analysis

With scanning electron microscopy (QUANTA 400F Field Emission SEM) examination, it was aimed to investigate the shape and morphology of the nanoparticles. Gold coating was conducted before SEM analysis in METU Central Laboratory (Ankara, Turkey).

For determination of diameter distribution of NPs, histogram images were formed by using ImageJ 1.x image processing program. Diameters of approximately 200 NPs were measured.

2.2.3.3. Zeta Sizer and Zeta Potential Measurements

During size measurements of the NPs by Zeta sizer (MALVERN Nano ZS90), the zeta potential measurements were also performed to determine the surface charge and

electrostatic potential on the surface of the nanoparticles in METU Central Laboratory (Ankara, Turkey).

2.2.4. Investigation of *in vitro* Biocompatibility: Cell Viability Tests of Heparin, and Heparin-Loaded Nanoparticles

L929 fibroblast cells were grown in high glucose-DMEM medium supplemented with 10% fetal bovine serum (FBS) and 1% Penicillin-Streptomycin solution. Cells grown on T-75 cell culture plates were passaged using trypsin-EDTA under sterile laminar flow when the cells reached 80% confluency. Cells were incubated at 37°C in an incubator with a humid atmosphere of 5% CO_2.

L929 cells were seeded to 96-well plate at a density of $1x10^4$ cells/well and incubated at 37 °C in carbon dioxide incubator. For dose dependent effect of heparin on cell viability different doses of free heparin (1-200 IU/ml) were added to each well and viability results of cells were determined after 24, 48 and 72 hours by using MTT cell proliferation reagent.

To the nanoparticle treated cells, a modified cell culture study was applied. Proliferation of cells treated with heparin loaded NPs and empty NPs was determined by using cell inserts (Figure 2.2). L929 cells (200000 cells/well) were seeded on 24 well plates and 5 mg heparin loaded nanoparticles or empty nanoparticles were placed on inserts. Measurement of cell viabilities was performed with Alamar Blue Assay at 24, 48 and 72 hours.

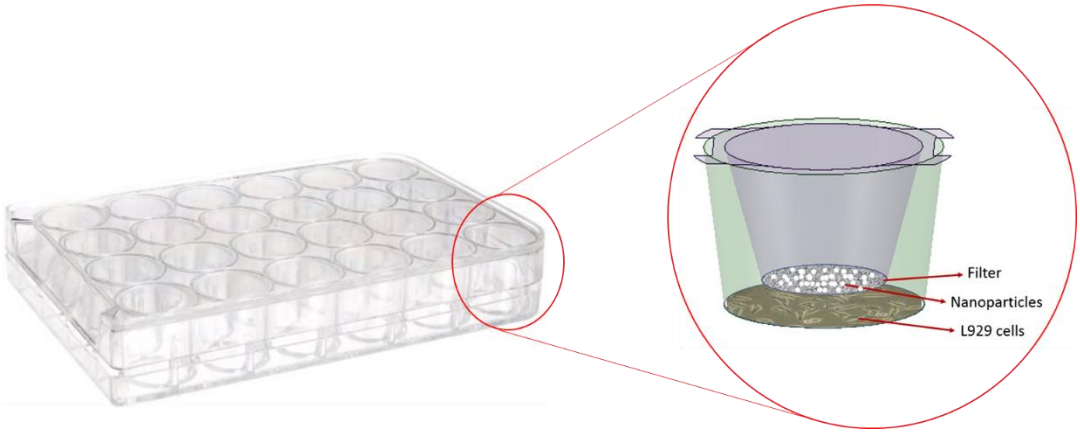

Figure 2.2. Illustration of cell viability analysis by using cell inserts

2.2.5. Preparation of Skin Tissue Engineering Constructs

2.2.5.1. Optimization of Electrospinning Process for Sericin/Gelatin Nanomats

In the preparation of skin tissue engineering construct and carrier of nanparticles, sericin and gelatin biopolymers were used. Polymer solutions were converted to fibrous matrices via electrospinning process. Shematic representation of wet electrospinning mechanism is given in Figure 2.3.

Electrospinning operation is based on the formation of electric field between the tip of syringe for pumping polymer solution and the collector, on polymer solution by high voltage source. Gamma High Voltage Source ES30 (Gamma High Voltage 25 Research, Inc., Florida, USA) was used for electrical field formation. Other materials were NE-1000 syringe pump (New Era Pump Systems, Inc., New York, USA) and plexiglass cabinet made up of Poly(methyl methacrylate) (PMMA).

Basically, after polymer solution was drawn into syringe, it was inserted in syringe pump. While power supply was connected to the needle of the syringe, aluminium foil covered collector was grounded for conventional electrospinning process (

Figure 2.4). Even though the experiments conducted in this study have begun with conventional electrospinning, because of easy collection of electrospun fibers from

collector containing liquid, the experiments were continued with the wet electrospinning.

Electrospinning set-up located in vertical position were preferred for wet electrospinning process. Fibers were collected on petri dish, that was filled with absolute ethanol, reside on custom-made rotational collector stand (Figure 2.5). Fabricated scaffolds were lyophilized via freeze-drier (Labconco Corporation, Kansas City, USA) after freezing at -80 °C for storage.

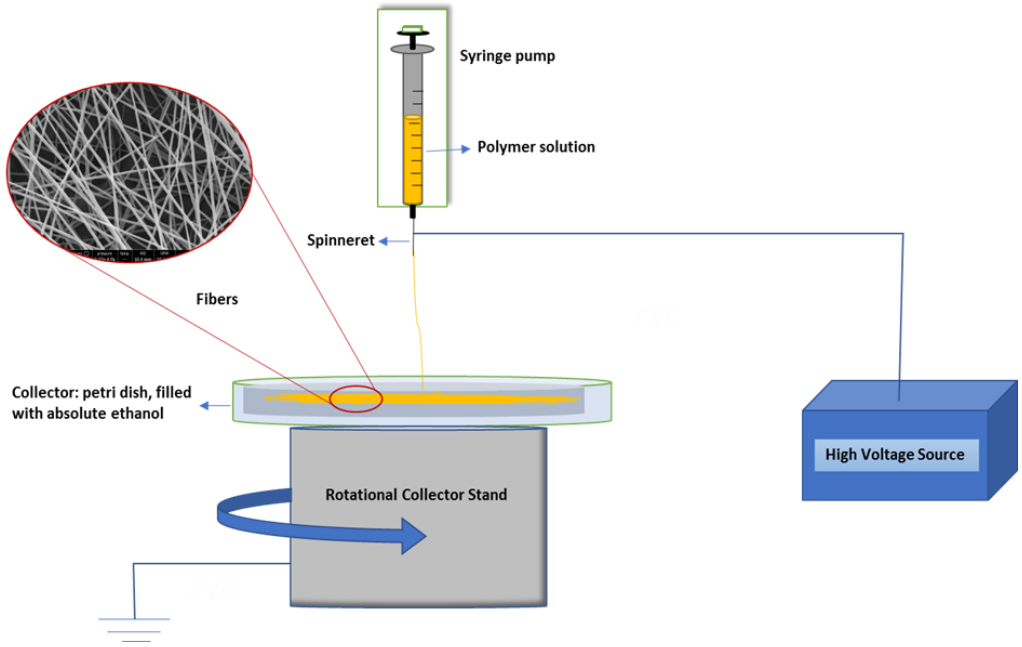

Figure 2.3.Shematic representation of wet electrospinning mechanism

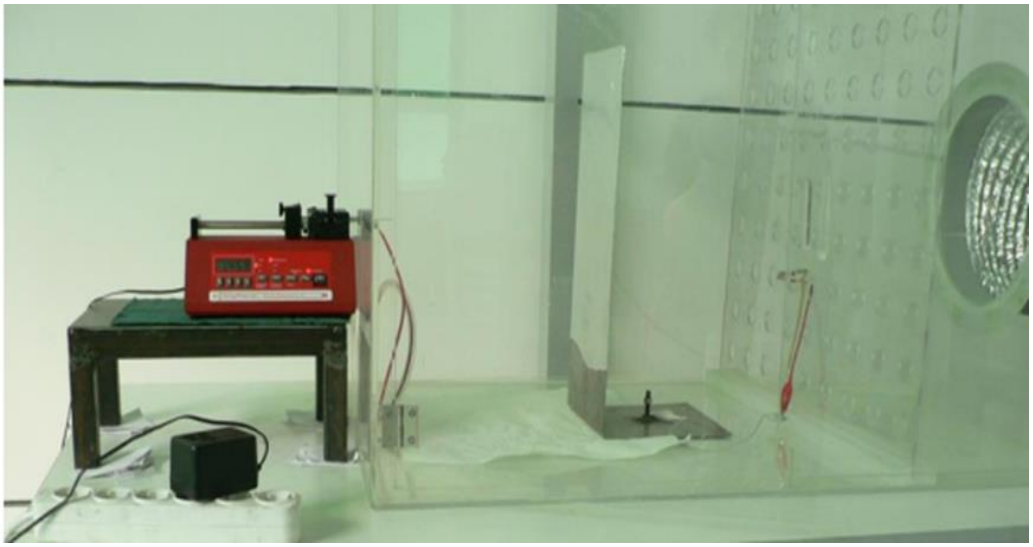

Figure 2.4. Conventional electrospinning set-up

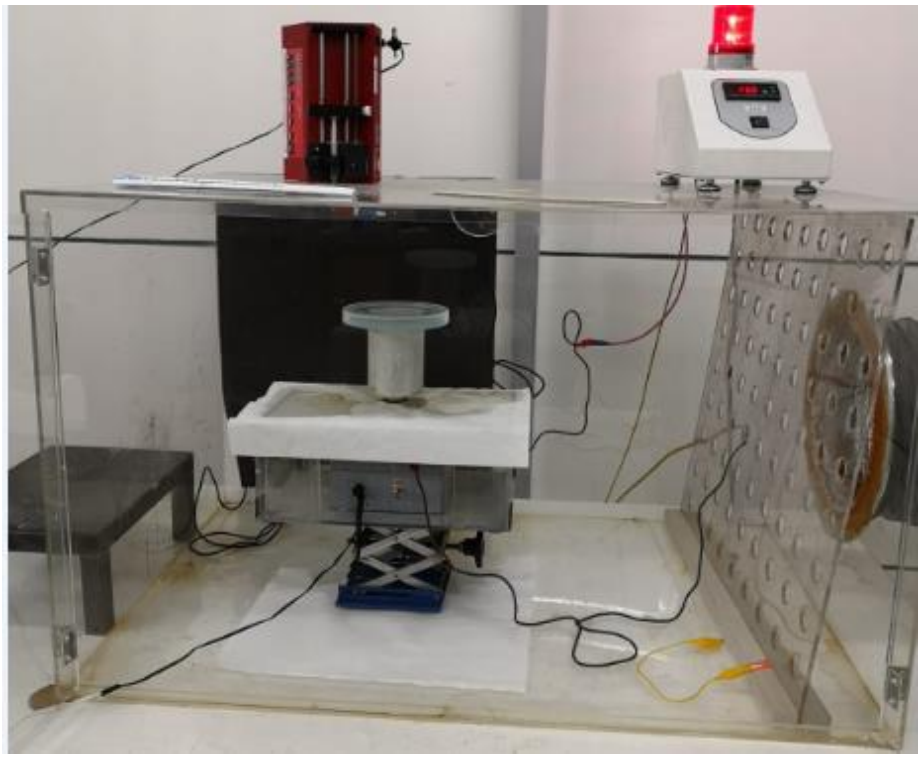

Figure 2.5. Wet electrospinning set-up

For optimization of electrospinning of sericin/gelatin solutions, different concentrations of both polymers were mixed to achieve optimum fiber conformation. Distilled water, 10% acetic acid and 20 % acetic acid were tested for conventional electrospinning (Table 2.1). For wet electrospinning studies, 10% acetic acid and 20% acetic acid and 20% acetic acid solution having 5% DMSO were used to dissolve both sericin and gelatin polymers. Table 2.2 shows the solutions that were investigated in sericin/gelatin electrospinning experiments.

Table 2.1. Composition and concentration of solutions that were tested in conventional electrospinning

Group No:	Solvent	Total Polymer Concentration (%) (w/v)	Sericin/Gelatin Ratio
1	Distilled water	20	1/1
2	Distilled water	30	1/2
3	Distilled water	30	2/1
4	Distilled water	40	2/1
5	Distilled water	40	3/1
6	10% Acetic acid	20	2/1
7	10% Acetic acid	20	1/2
8	20% Acetic acid	20	1/2
9	20% Acetic acid	20	2/1
10	20% Acetic acid	20	0/1

Table 2.2. Composition and concentration of solutions that were tested in wet electrospinning

Group No:	Solvent	Total Polymer Concentration (%) (w/v)	Sericin/Gelatin Ratio (w/w)
1	10% Acetic acid	20	1/2
2	20% Acetic acid	20	0/1
3	20% Acetic acid	20	1/2
4	20% Acetic acid 5% DMSO	10	1/2
5	20% Acetic acid 5% DMSO	20	2/1
6	20% Acetic acid 5% DMSO	20	1/2
7	20% Acetic acid 5% DMSO	20	0/1
8	20% Acetic acid 5% DMSO	20	1/7
9	20% Acetic acid 5% DMSO	20	1/3

The best solvent system for electrospinning of Sericin:Gelatin polymer mixture was determined as 20% Acetic Acid and 5 % DMSO containing aqueous solution. 20 wt % was chosen as a total polymer concentration for fibrous matrix formation. For the following experiments, it is decided to continue with groups having Sericin/Gelatin ratio 0:1, 1:2, 1:3 and 1:7. Optimum electrospinning conditions for selected groups were determined with several trial of different parameters on group having 1:2 Sericin/Gelatin ratio which were voltages (kV), syring pump rates (mL/hr) and spinneret and collector distances (cm) (Table 2.3).

Table 2.3. Electrospinning conditions for selected polymer concentration

Condition No	Voltage (kV)	Rate (mL/hr)	Distance between spinneret and collector (cm)
1	15	2	10
2	18	2	10
3	20	2	10
4	20	3	10
5	20	4	10
6	20	2	15

2.2.6. Preparation of Nanoparticle loaded Gelatin/Sericin Skin Tissue Engineering Constructs

HP loaded nanoparticles were incorporated into fiber stuctures of scaffolds by adding them in gelatin/sericin solution before electrospinning. Distilled water, 10 % acetic acid and 20 % acetic acid and 20 % acetic acid solution having 5 % DMSO solvents that were used in optimization studies of polymer electrospining were also tested to check dissolution of heparin loaded PLGA nanoparticles as this might disturb final aimed design of the scaffolds.

Loading of nanoparticles in fibers were performed by adding newly synthesized NPs after washing and resuspending in distilled water to the polymer solution at a weight of 20%. The best conditions for electrospinning of nanoparticle incorporated gelatin/sericin aquous solution were decided according to previous observations on sericin/gelatin nanomats production.

2.2.7. Crosslinking of Scaffolds

Basically, aldehyde group in GTA is reactive towards ε-amino groups of lysine residues of proteins. Therefore, aldimine linkage (CH=N) formation occurs after GTA crosslinking (Nguyen & Lee, 2010).

Crosslinking with glutaraldehyde (GTA) was performed since gelatin and sericin are water-soluble materials. All Ser/Gel samples were weighed before immersing to crosslinker solution. GTA solution was prepared at 5 % concentration in water. The samples were exposed to 5 % GTA for 2 hours.

2.2.8. Characterization of Scaffolds

2.2.8.1. Scanning Electron Microscopy (SEM)

SEM was used to investigate the morphology of scaffolds. Fiber homogeneity in terms of size and shape and their diameters were determined using SEM examination of selected groups. Scaffold structures were examined by Quanta 400F Field Emission SEM device (FEI, USA) between 500 V and 30 kV in Central Laboratory at METU (Ankara, Turkey). Gold coating was performed before the analysis.

2.2.8.2. Fourier Transform Infrared Spectroscopy Analyses

FTIR analyses were performed to investigate incorporation of NPs into scaffolds by Bruker IFS 66/S in Central Laboratory at METU (Ankara, Turkey). The analysis was performed in wavenumber range 400- 4000 cm^{-1}, with a resolution of 4 cm^{-1}.

2.2.8.3. Degradation Study

For degradation studies, selected groups of NP incorporated and not incorporated scaffolds (n=3) were cut into pieces with 5 mg weight and each was incubated in 2 mL phosphate buffered saline (PBS, 0.1 M, pH 7.2) solution at 37°C in water bath (Nüve Bath NB 5, Turkey) for 7 days. To determine the weight loss in the PBS solution, dry weights of the samples were determined at the end of each time period (1, 3, 7, 14 and 21 days).

Weight loss percentages were calculated using the formula;

$$\text{Weight loss \%} = \frac{Wt - Wi}{Wi} \text{ x100}$$

W_t; dry weight of scaffold at time point, t (g)

W_i; initial weight of the scaffold (g)

2.2.8.4. Water Absorption Analysis

General gravimetric method was used to determine water absorption of constructs (Akturk et al., 2011). The preweighed scaffold pieces (5–8 mg) were immersed in PBS (pH 7.4, 0.1 M) and incubated at 37 ºC water bath (Nüve Bath NB 5, Turkey). At 1st, 3rd and 7th days, scaffolds were removed from the PBS and excess liquid on them was eliminated by touching filter paper and wet weight of the membranes were measured. The swelling degree was calculated by using following formula (Tanodekaew et al., 2004);

$$\text{Swelling Degree} = \frac{W_w - W_d}{W_d}$$

W_w= wet weight of scaffold

W_d= dry weight of scaffold

2.2.9. Heparin Release Studies from Scaffolds

Release analysis were performed with 5 mg NP loaded scaffolds having 0/1 and 1/2 Ser/Gel ratio. Samples were placed into a dialysis membrane with 14,000 molecular weight cut off. Scaffold dialysis was performed against 2 mL PBS (pH = 7.4, 0.1 M) solution by stirring it at 37°C in a water bath. Release samples were taken at the same time periods as the release results taken from NPs (1, 2, 6, 12, 24 48, 72 and 168 hours).

The amount of released heparin was calculated from the standard curve of heparin in PBS (pH 7.4, 0.1 M) by using DMMB assay.

2.2.10. Cell Viability Assays for Constructs on Fibroblast Cell Line

L929 fibroblast cells were grown in DMEM medium supplemented with 10% fetal bovine serum (FSS) and 1% penicillin-streptomycin solution. Cells culture conditions were carried out as explained before in Section 2.2.4.

Cell attachment and proliferation on scaffolds were determined by Alamar Blue Assay (Invitrogen, USA). It is based on reduction of Alamar Blue, or resazurin salt with cellular metabolic activities. Reduced form of it is called resarufin which is excessively fluorescent and indicate cell viability quantitively.

Before cell viability analysis, NP-incorporated scaffolds were sterilized with alcohol and UV light exposure for one hour for each site. Scaffolds (n=3) were cut into pieces of 4 mm in diameter and placed on non-treated 96 well plates. Cells were seeded on scaffolds at a concentration of $1x10^4$ cells/scaffold. After cells seeded on scaffolds, they were incubated in a carbon dioxide incubator (37°C, 5% CO_2) (Shel Lab 5215, California, U.S.A.). As a control groups, scaffolds having 1:2 and 0:1 Ser:Gel ratio were analyzed for cell viability measurements.

Cell viability analyses with Alamar blue were performed at the end of 1^{st}, 3^{rd}, and 5^{th} days of incubation. To perform Alamar Blue assay, the cell culture medium was removed, and the scaffolds were washed with PBS (0.1 M, pH 7.4). Alamar blue solution (10% alamar blue and 90% DMEM without phenol red) was added to each well and incubated at dark for 4 hours. Absorbances of reduced solutions were obtained at 570 nm and 600 nm via microplate reader (SpectraMax iD3 Multi-Mode Microplate Reader, USA). As negative control, cell culture media containing alamarBlue was taken.

Percentage reduction of Alamar Blue can be calculated as indicated below formula;

$$\text{Percent reduction} = \frac{(O_2 * A_1) - (O_1 * A_2)}{(R_1 * N_2) - (R_2 * N_1)} * 100$$

Where;

O_1; molar extinction coefficient (E) of oxidized alamarBlue (Blue) at 570 nm

O_2; E of oxidized alamarBlue (Blue) at 600 nm

R_1; E of reduced alamarBlue (Red) at 570 nm

R_2; E of reduced alamarBlue at 600 nm

A_1; absorbance of test wells at 570 nm

A_2; absorbance of test wells at 600 nm

N_1; absorbance of negative control well (cell culture media containing alamarBlue but no cells) at 570 nm

N_2; absorbance of negative control well (cell culture media containing alamarBlue but no cells) at 600 nm

2.2.10.1. Scanning Electron Microscopy (SEM)

Determination of morphology of cells seeded on the 0/1 and 1/2 Ser/Gel ratio having scaffolds SEM analysis were performed. Before gold coating for SEM analysis, cell fixation protocol should be performed.

Exposure to 4 % paraformaldehyde was performed to form crosslink between proteins of cells and surroundings for 20 min. at room temperature. After crosslinking, ethanol dilution series were applied between 30% and 100% for 10 min. each to get rid of lipids and dehydrate the samples. For final dehydration of samples, scaffolds were

immersed in hexamethyldisilazane (HMDS) for 20 min. (Jusman, Ng, & Abu Osman, 2014). Samples were waited at 4 °C, until SEM analysis.

2.2.11. Statistical Analysis

Two- way analysis of variance (ANOVA) followed by Tukey's comparisons test was performed to compare results for the significant differences between groups by using GraphPad Prism version 8.00 for Windows (California USA).

CHAPTER 3

RESULTS AND DISCUSSION

3.1. Optimization Studies for Nanoparticle Synthesis

The first trial for NP synthesis were performed with homogenizer. The first emulsion was performed with 200 µl heparin solution and 2 ml 5% PLGA/DCM at 10000 rpm and in second emulsion 5% PVA was added to this mixture. Figure 3.1 shows the SEM image of the prepared particles. Microparticles were obtained with homogenizer. The sizes of the particles were between 185 nm and 4100 nm. Size of particles was not uniformly distributed.

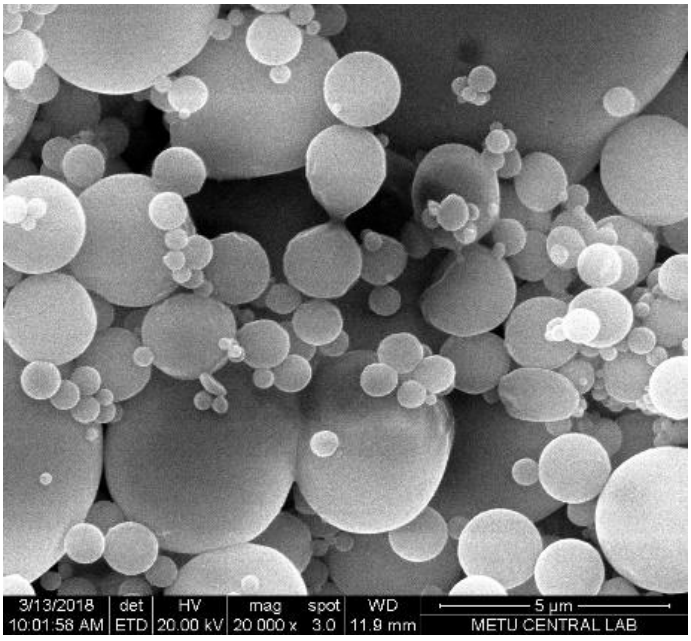

Figure 3.1. SEM image of NPs synthesis with homogenizer

For the preliminary studies, 100 mg PLGA or PCL was dissolved in 2 mL DCM. PLGA and PCL nanoparticle preparation were tried with sonicator (Figure 3.2). 5% PVA was used as a surfactant and sonicator amplitude was arranged to 10%. 1st and

2nd emulsions lasted 60 and 90 sec, respectively. As a result, micro-sized particle formation was observed in PLGA case (Figure 3.2.a), however, PCL particles were difficult to distinguish and they had an aggregated appearance (Figure 3.2.b). PCL particles were presenting a wider range of size distribution compared to PLGA ones. Besides, there were some parts where particle fusions had occurred. This might be due to low Tg of PCL which might have affected the outcome as the result of local changes in the heat during sonication step in particle preparation.

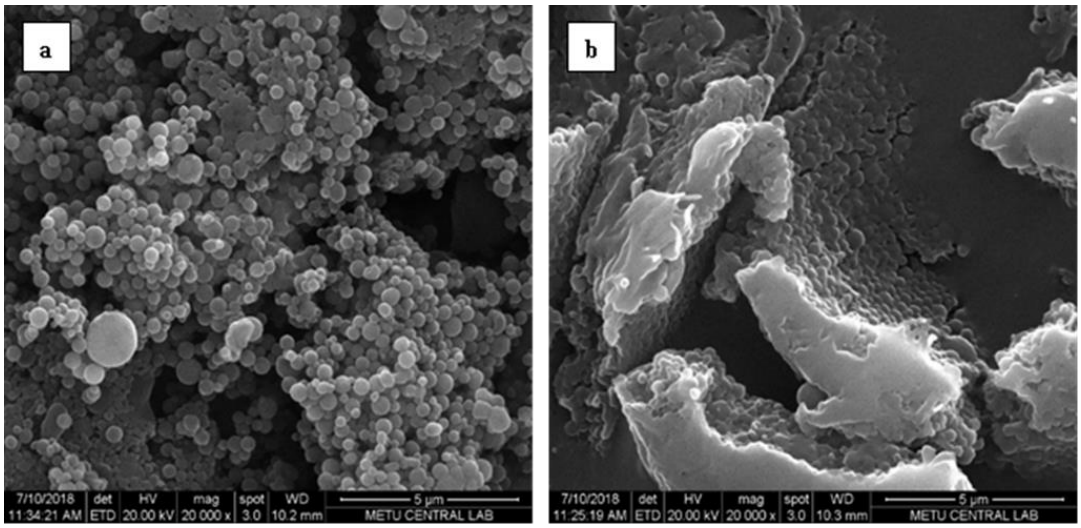

Figure 3.2. PLGA (a) and PCL (b) particle synthesis with probe sonicator

To get much lower sized NPs the concentration of the PVA was declined to 3% from 5% for second emulsion preparation step and 10 and 20% amplitudes were tested. Apparently, SEM images in Figure 3.3 showed that NP sizes were smaller at 20% amplitude because amplitude is directly related to intensity of the sonication and increase in intensity of sonication lead to smaller sized NP formation (Sussman & Bates-Jensen, 2012).

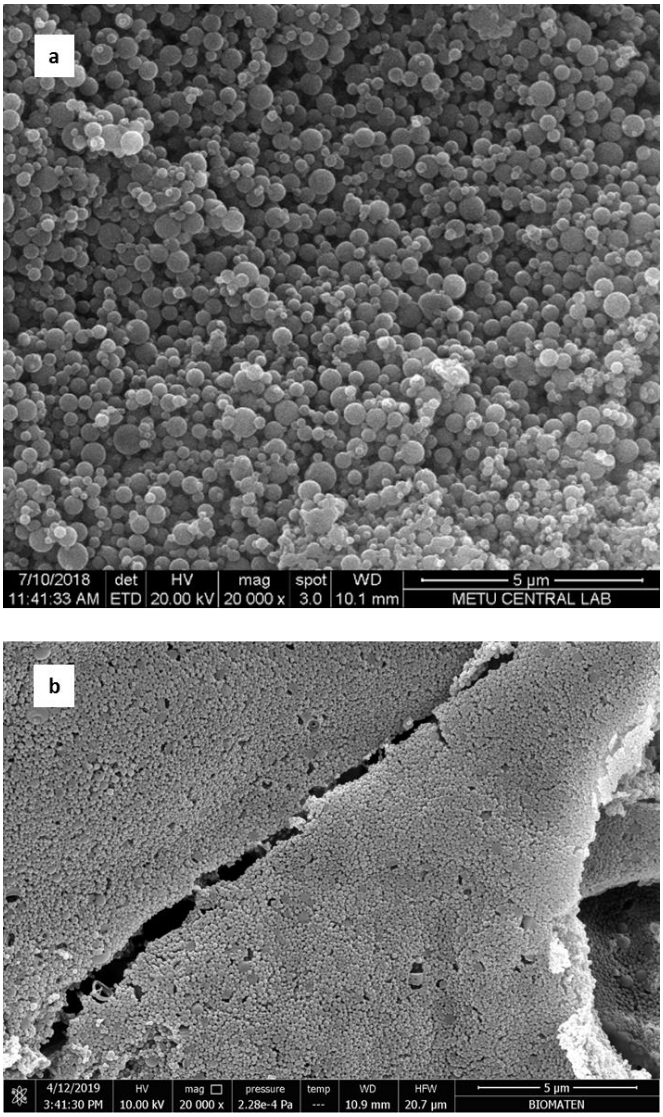

Figure 3.3. SEM images of NPs synthesized with 3% PVA as a surfactant with amplitudes 10% (a) and 20% (b) by sonicator

3.2. Properties of Heparin-Loaded Polymer NPs

3.2.1. Chemical Properties

Chemical composition of heparin-loaded and unloaded NPs, and heparin were determined with infrared spectroscopy (Figure 3.4). The strong stretching band between 1770 and 1750 cm^{-1} was assigned to carbonyl groups (C=O) in lactide and glycolide units of the PLGA. Bands between 2885 and 3010 cm^{-1} were attributed to

C-H stretches in the PLGA (Gurpreet et al.,2014). The absorption band located in the 1094.5 cm^{-1} shows the C-O stretches and C-H bends were observed between 1450-850 cm^{-1} at unloaded NPs and heparin-loaded NPs. Bands at 1236 cm^{-1} were attributed to S=O groups of heparin and at the 890 cm^{-1} assigned as C-O-S bond in the molecule structure of heparin (Martins et al., 2012).

Heparin loaded NPs and unloaded NPs showed similar IR spectra. Different functional groups and chemical bonds were not observed between these spectra. This shows that the polymer does not interact with heparin to form a new bond.

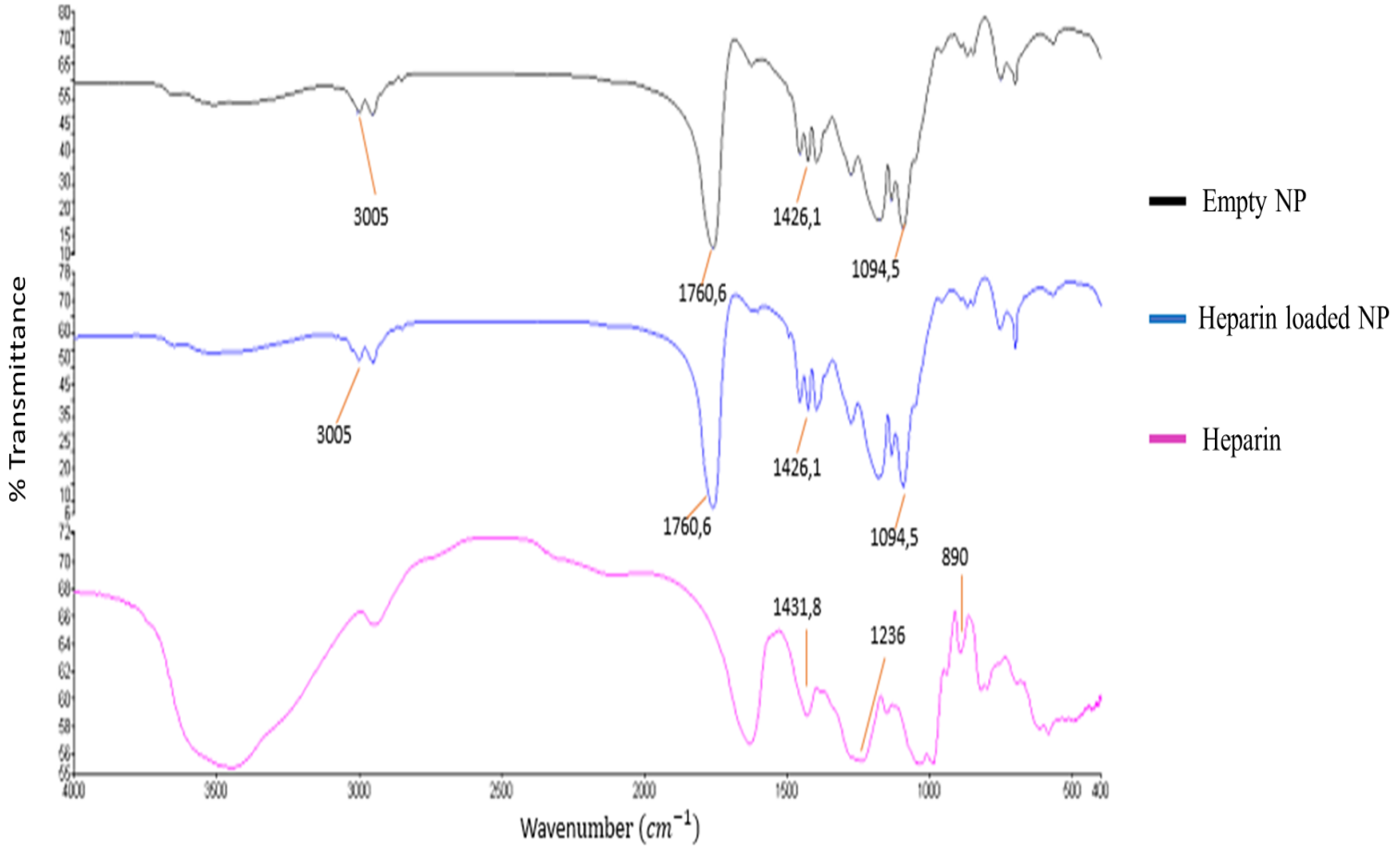

Figure 3.4. FTIR spectra of empty NP, heparin loaded NP and heparin

3.2.2. Morphological Properties

Size and morphology of unloaded NPs and Heparin loaded NPs were examined by SEM (Figure 3.5). Both NPs had uniform size distribution and shape. Surface of NPS were quite smooth and showed no deformations.

According to SEM images, presence of HP in the inner phase of NPs resulted in increase of average NP diameter. The reason of this may be water retention capability of HP, resulting in larger polymer sphere formation during NP production.

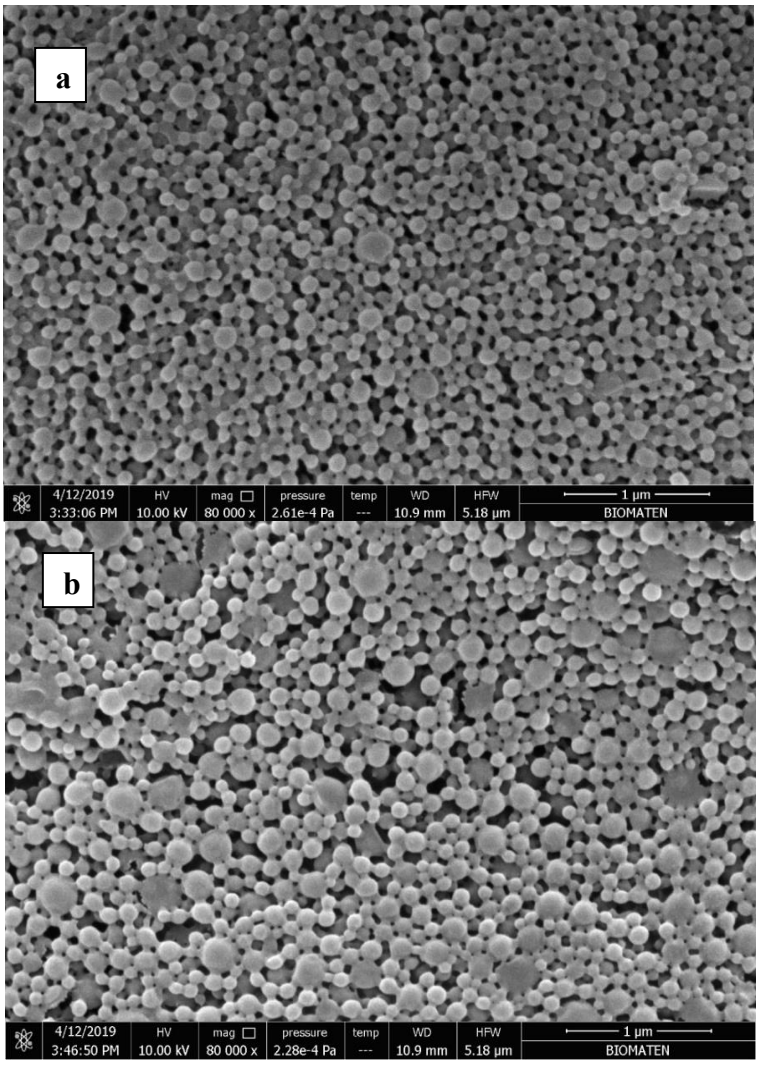

Figure 3.5. SEM images of unloaded NPs (a), Heparin-loaded NPs (b)

Histogram images were formed by using ImageJ 1.x image processing program to compare zeta sizer results and SEM images (Figure 3.6).

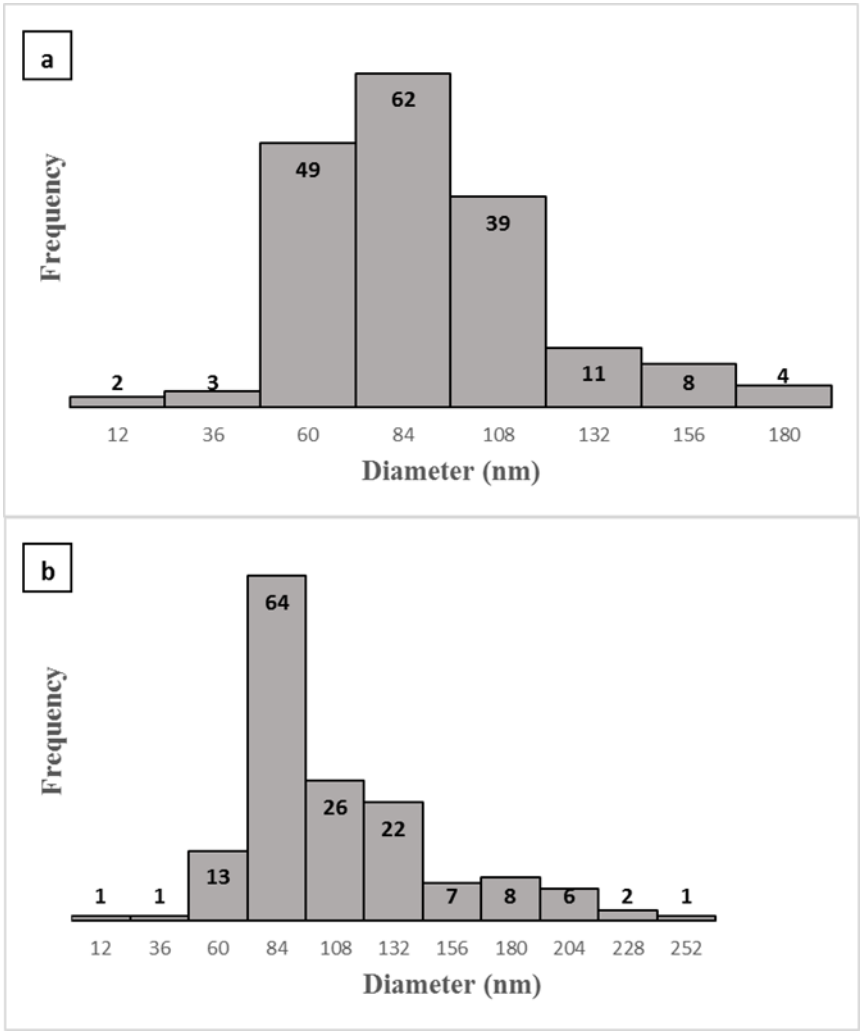

Figure 3.6. Histogram for particle sizes obtained in SEM images for bare NPs (a), Heparin-loaded NPs (b)

3.2.3. Zeta Sizer and Zeta Potential Measurements

The results of Dynamic light scattering (DLS) analysis showed the average size of unloaded NP was 269.4 nm and size of HP loaded NPs as nearly 207.7 nm (Figure 3.7). However, SEM observations point out average sizes of NPs as 89.39 ± 30.67 nm and 109.74 ± 44.03 for unloaded NPs and HP loaded NPs, respectively (Figure 3.6).

Eaton et al. showed the comparison of DLS data and SEM images of the silica nanoparticles in terms of particle sizes. The silica samples gave smaller particle size in microscopy (nearly 50 nm) compared to studies in DLS (nearly 140 nm). This result was attributed to dynamic behavior of particles rather than the individual particle size. Because of the non-stable distribution of particles in the solution, particles should be dispersed by mixing well (Eaton et al., 2017).

In this study, the reason of the conflict between SEM and DLS analysis might be agglomeration of NPs in aqueous environment during analysis with zeta sizer. SEM images were taken after samples freeze dried, to get zeta sizer results freeze dried NPs were resuspended in distilled water. Even though NP solution in water was stirred vigorously, apparently NP agglomerations were identified with zeta sizer.

PLGA NPs which were prepared by PLGA (50:50) with double emulsion solvent evaporation method by using 5% of PVA as a surfactant showed average particle size between 156 and 197 nm (Hussein, Fakhru'l-Razi, & Abdullah, 2013). The PLGA particle size was determined with DLS as 232.57 ± 10.56 nm in another study by using 0.2% PVA with the same method (Chen & Wen, 2018).

a

		Diam. (nm)	% Intensity	Width (nm)
Z-Average (d.nm): 269,4	Peak 1:	346,7	100,0	212,4
PdI: 0,177	Peak 2:	0,000	0,0	0,000
Intercept: 0,950	Peak 3:	0,000	0,0	0,000
Result quality Good				

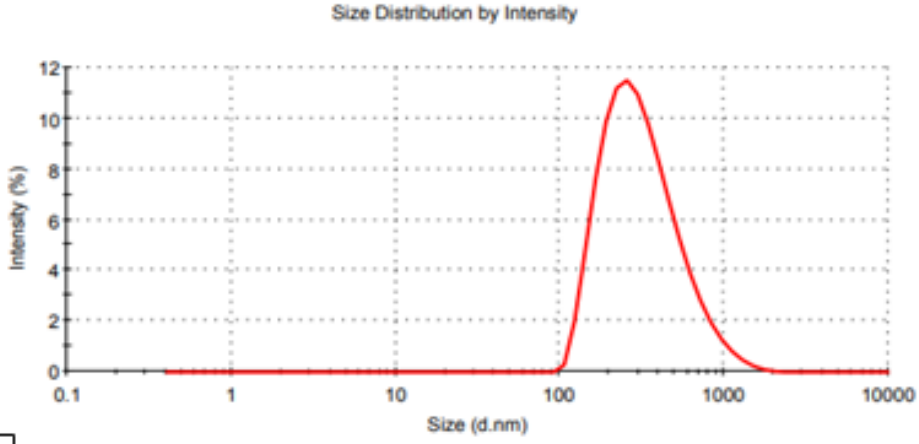

b

		Diam. (nm)	% Volume	Width (nm)
Z-Average (d.nm): 207,7	Peak 1:	240,5	100,0	124,6
PdI: 0,128	Peak 2:	0,000	0,0	0,000
Intercept: 0,936	Peak 3:	0,000	0,0	0,000
Result quality Good				

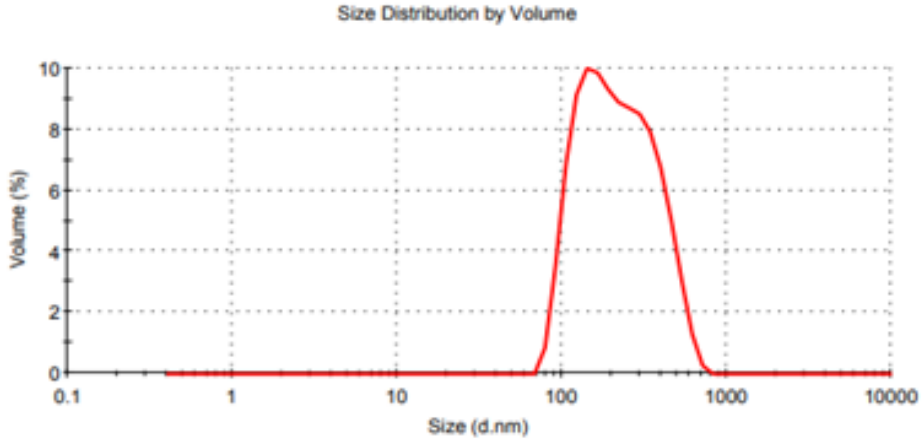

Figure 3.7. Zeta sizer analysis for empty NPs and HP loaded NPs

Zeta potential is the electric potential between interface of dispersed particles and a stage in the continuous phase remote from interface (Lu & Gao, 2009). It provides data on particle charging and the desire of particles to combine or to be separate. The zeta potential measurements were also performed by Zetasizer to determine the surface charge and electrostatic potential on the surface of the nanoparticles and to examine colloidal stability (Gupta & Trivedi, 2018). Examined results of empty NPs and HP-loaded NPs zeta potentials were determined as -23,9 and -20,9 mV, respectively (Figure 3.8). For the monodistribution of NPs, values more positive or negative than 30 mV zeta potential is desired. Colloids having zeta potential values between 10 and 30 mV, is considered as they have incipient stability. Much lower zeta potential values (< 10 mV) can lead to agglomeration of NPs (Pate & Safier, 2016). Accordingly, both of the empty NPs and HP-loaded NPs have had incipient stability in this study.

Zeta potential values of PLGA nanoparticles prepared with PLGA (50:50) changed from -26 to -28 mV and it is claimed that these results are indicating relative stability of PLGA NPs in emulsions (Hussein et al., 2013). -16.4 ± 0.23 mV zeta potential value was determined for PLGA NPs prepared with single emulsion solvent evaporation method (Tansik, Yakar, & Gündüz, 2014).

a

		Mean (mV)	Area (%)	Width (mV)
Zeta Potential (mV): -23,9	Peak 1:	-23,9	100,0	6,36
Zeta Deviation (mV): 6,36	Peak 2:	0,00	0,0	0,00
Conductivity (mS/cm): 0,0234	Peak 3:	0,00	0,0	0,00

Result quality Good

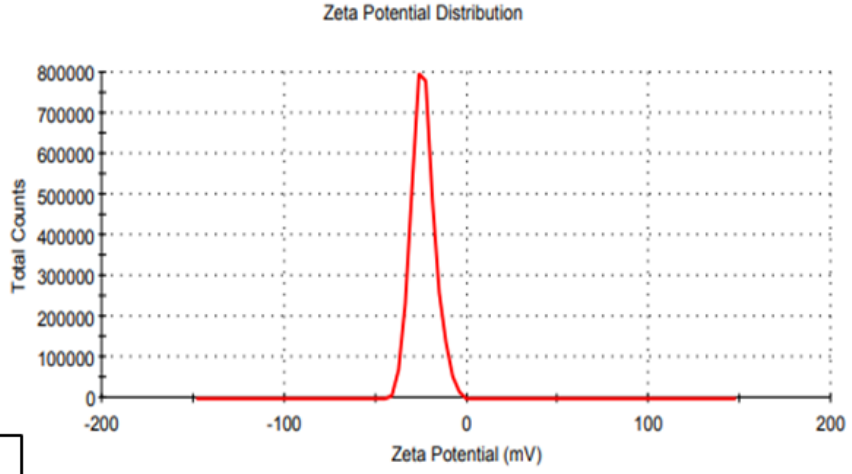

b

		Mean (mV)	Area (%)	Width (mV)
Zeta Potential (mV): -20,9	Peak 1:	-20,9	100,0	5,72
Zeta Deviation (mV): 5,72	Peak 2:	0,00	0,0	0,00
Conductivity (mS/cm): 0,00913	Peak 3:	0,00	0,0	0,00

Result quality Good

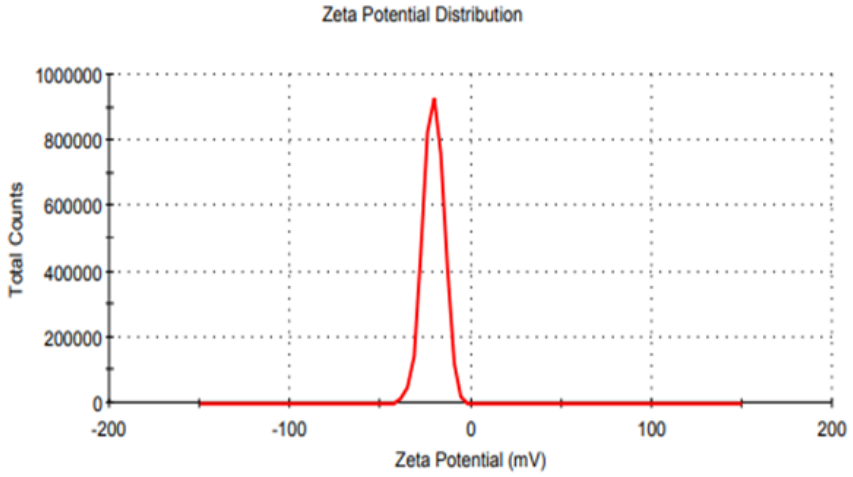

Figure 3.8. Zeta potential measurements for bare NPs (a), Heparin-loaded NPs (b)

3.3. Heparin Loading and Encapsulation Efficiency Results

Heparin loading and encapsulation efficiencies of NPs were determined indirectly. DMMB calibration curve in distilled water used for determination of HP content was given in Figure A. 1. In this study use of DMMB method, which is used for detection of other GAGs, was modified and developed for the first time for Heparin detection. During literature survey it was recognized that there is no established method or experimental research on quantitative analysis of heparin for *in vitro* studies.

Encapsulation efficiency of HP-loaded NPs was determined as 60.9% and loading capacity of them was 30.04 mg/g of polymer (5478.7 IU/g of polymer). In this study, much higher loading capacity was gained compared to results obtained by Jiao et al. (2002), that was 2792 IU HP loading per gram of PLGA NPs.

The two previous studies which are related to HP loading to biodegradable (PCL and PLGA) and non-biodegradable polymers (Eudragit RS and RL) showed encapsulation efficiencies for the PCL NPs as 16% and 8%, and for the PLGA NPs as 10.6% and 14%, respectively. (Hoffart et al. 2002, Jiao et al. 2002).

3.4. Heparin Release Profiles of Nanoparticles

The amount of released heparin was calculated from the standard curve of heparin in PBS by using DMMB assay (Figure A. 1).

Generally, it is expected to come out of drug on the surface or close to surface easily in the first 6 hours, because of the burst release of drug from the surface. Then, the molecules loaded to inside of NPs are expected to be released slower and more controlled manner (Freiberg & Zhu, 2004).

For controlled release studies, both the solubility and the diffusibility of the active molecule (HP) are important. The release of loaded agent from the PLGA NPs occurs through the pores by diffusion since the polymer carrier cannot be expected to degradation in such a time.

Release samples were taken at 1, 2, 6, 12 and 24 hours for the first day and the other measurement made second, third and seventh days. First 6 hours results were taken to see the initial burst release. To observe the controlled release pattern, release profile was examined 12 and 24 hours as well.

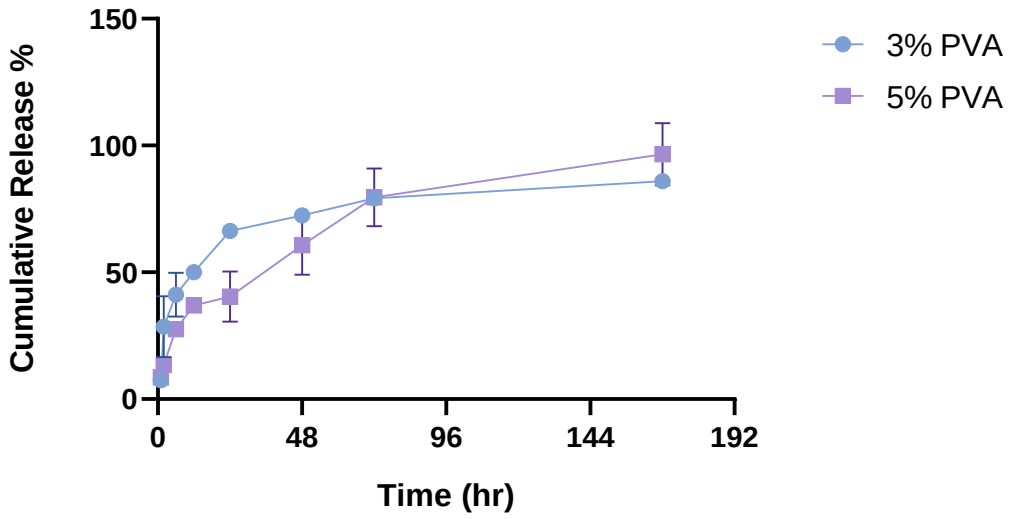

Figure 3.9. Cumulative release of heparin from HP-loaded PLGA NPs. The data are represented as the mean ± Std. (n = 3).

The cumulative release profiles of the heparin from PLGA NPs prepared with 3% and 5% PVA are given in Figure 3.9. The release study was continued up to 7 day. Nearly 65% of HP was released within first 24 h from the NPs prepared with 3% PVA. Although approximately 30% of release was burst release of HP in the first two hours, HP release continued in a slower manner in time. However, NPs prepared with 5% PVA showed approximately 40% HP release in first 24 hr. Since the size of NPs synthesized with 3% PVA was in nanoscale, the experiments were continued with these ones.

Hoffart et al. (2002) examined low molecular weight heparin (LMWH) release from PCL and PLGA (50:50) NPs and also from the NPs composed of combination of PCL and PLGA polymers with non-biodegradable positively charged polymers (Eudragit RS and RL) by using indirect detection method with cetylpyridinium solution for oral

drug delivery. PCL and PLGA NPs showed nearly 25 % and 20 % release at the first day. And the highest release percentages were obtained in the single biodegradable polymer containing groups (Hoffart et al., 2002). Contrarily in another study, from the Chitosan–hyaluronic acid NPs, unfractionated HP and low molecular weight heparin (LMWH) showed 10.8% HP and 79.7% LMWH release within 12 hr of incubation. This very slow release of UFH was suggested to be because of the g electrostatic interaction between positively charged chitosan and high net negatively charged heparin (Oyarzun-Ampuero et al. 2009).

In this thesis study, this release profiles were quite unexpectable considering hydrophobic nature of PLGA and the results of similar studies (Kim & Martin, 2006). However, due to high water solubility and water retention capacity of HP this outcome was reasonable, besides large surface to volume ratio aspect of NPs provide more interaction with aqueous environment and larger surface area for release.

3.5. Investigation of *in vitro* Biocompatibility: Cell Viability Tests of Heparin, and Heparin-Loaded Nanoparticles

Cell viability analysis of HP exposed cells was performed with MTT assay. However, cell viability analysis of HP loaded PLGA NPs treated cells was performed by Alamar Blue assay on L-929 mouse fibroblast cell line.

Cells were treated with free HP for 24, 48 and 72 hr in 96- well plates to observe the proliferative effect of HP on fibroblast cells. According to MTT results, all doses, from 1 IU/ml to 200 IU/ml, resulted in higher cell viability compared to cell control which was non-treated cells that were accepted as having 100% cell viability in calculations (Figure 3.10). MTT results showed that cells had similar viabilities in experimental groups (approximately 80%) compared to controls in 24 hours but cell viabilities increased with time. Cell viability of L929 cells at 72 hr was much higher than that of at 48 hr. Cells exposed to doses between 1 and 25 IU/ml HP showed significantly higher proliferation compared to control cells. However, the highest proliferation was determined on cells treated with the lowest HP concentrations (1 and 5 IU/ml).

In a previous study to investigate HP toxicity in cell culture, 10 different doses (10–300 units/well) of heparin were applied to L929 cells on 96 well plates by MTT assay. Increase in concentration of heparin led to a significant decline in cells viability for doses higher than 40 IU/well at first day, and 150 IU/well for second and third days (Gurbuz et al. 2013). Since we prepared our highest dose of heparin as 200 IU/well, there was no toxic effect of heparin in the concentration range in our experiments.

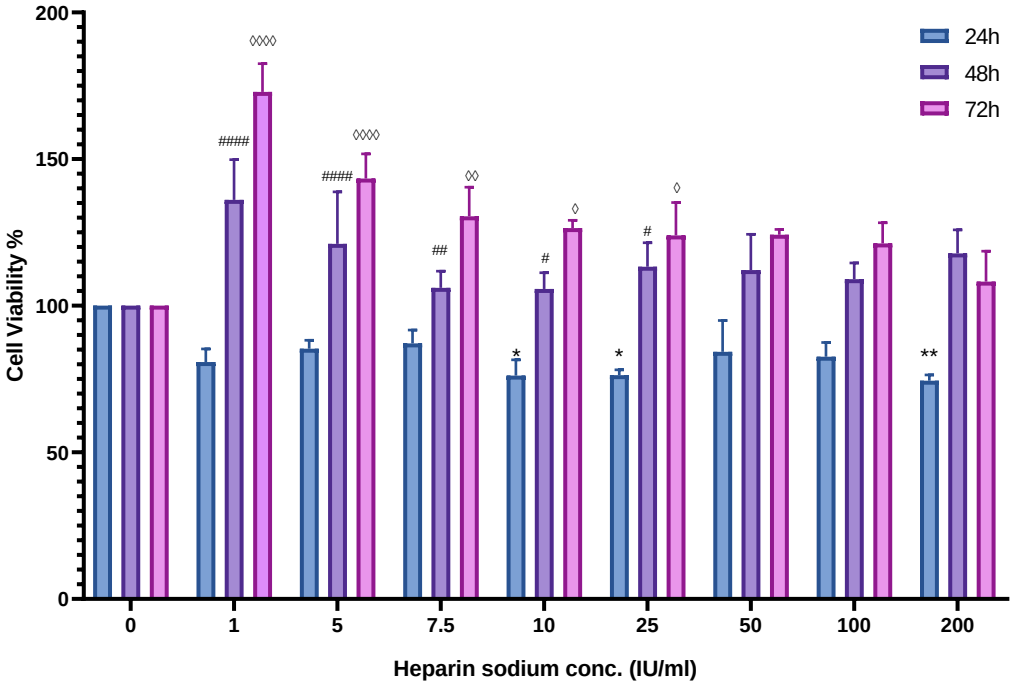

*Figure 3.10. MTT analysis for heparin treated L-929 cells. The data are represented as the mean ± Std. (n = 3). Proliferation of control cells was taken as 100%. ◊, # and * show significant difference of HP exposed cells from control cells. Two-way ANOVA with Tukey's comparison test ($p<0.05$) was performed.*

For NP cytotoxicity experiments, 5 mg NP was added on cell culture inserts and then cell viability analysis was conducted with Alamar Blue for 3 different time periods (24, 48 and 72 hrs) (Figure 3.11). In this study, 27.4 IU heparin was loaded to 5 mg NP. It is obviously seen that biodegradable PLGA NPs do not have any cytotoxic effect on L-929 cells. Statistical analysis performed with two-way ANOVA with Tukey's comparison test ($p<0.05$) did not show significant difference between cells exposed to HP-loaded NPs and unloaded NPs.

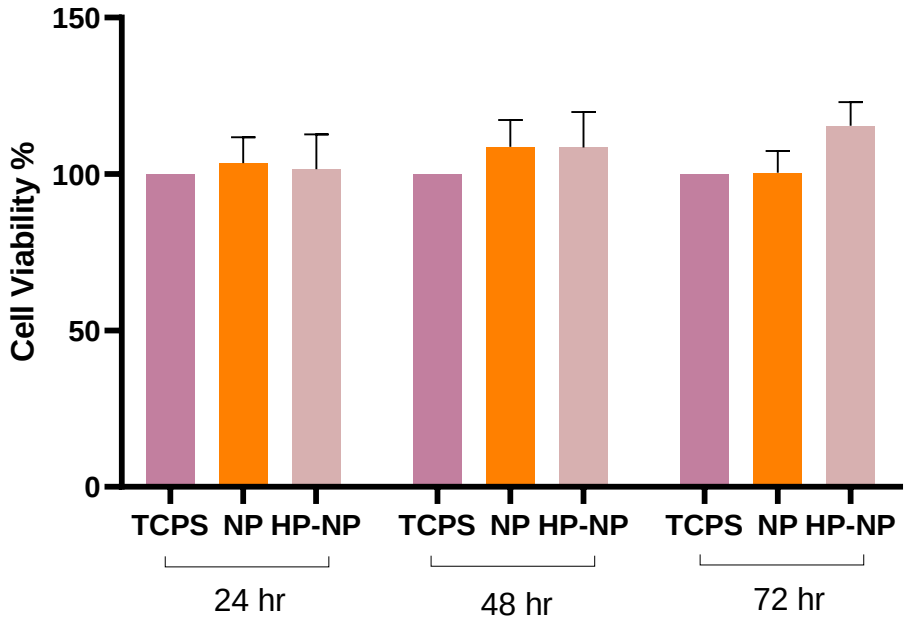

Figure 3.11. Effects of bare NPs and HP-loaded NPs on viability of L-929 cells. The data are represented the mean ± Std. (n = 3). Proliferation of control cells was taken as 100%. Two-way ANOVA with Tukey's comparison test ($p<0.05$) was performed.

3.6. Optimization Studies for Skin Tissue Engineering Constructs

For determination of the solvent system for electrospinning of Sericin/Gelatin polymers, several solvents were used in optimization studies. Conventional electrospinning and wet electrospinning methods were tried to get proper and applicable scaffold forms.

3.6.1. Conventional Electrospinning of Sericin/Gelatin Scaffolds

Wound dressings were prepared by using conventional electrospinning method at first. During optimization studies of electrospinning process, solvent type and concentration, total polymer concentration and sericin/gelatin ratio were changed. For conventional electrospinning, distilled water and acetic acid solutions having 5%, 10% and 20% concentrations were tested as solvent. At polymer concentration lower than 20%, fiber formation was not observed and at higher concentrations, blockages at the syringe tip occurred. Therefore, experiments continued with polymer solution having

20% (w/v) polymer concentration. Sericin/gelatin ratio was arranged as 0/1, 1/1, 2/1 and 1/2 (w/w) for conventional electrospinning trials.

The most suitable electrical voltage, flow rate, and distance between the needle tip and the collector surface were tuned and determined by arranging the variables between the intervals; 15-25 kV, 1-4 ml/hr, and 10-30 cm, respectively.

3.6.1.1. Characterization of Conventionally Electrospun Sericin/Gelatin Scaffolds with SEM

For determination of fiber morphology, diameter and conformation at different conditions, such as solvent concentrations and polymer ratios, SEM analyses were performed. These scaffolds were examined on the aluminum surface which was used as the collector surface during electrospinning experiments.

SEM images of various groups and optimization conditions are illustrated in Figure 3.12. There was no fiber formation when the polymers were dissolved in distilled water (Figure 3.12.a). Irregular aggregates and beads were obtained because it was hard to get fibrous structure by using water as a solvent in electrospinning due to its high surface tension (Kny, Ghosal, & Thomas, 2018). Bead formation decreased in accordance with increase in acetic acid amount in the solvent system (Figure 3.12.d). and there was no significant change in fiber diameter. Concentrations higher than 20% acetic acid were not preferred due to the possibility of dissolution of PLGA nanoparticles during electrospinning of NP loaded polymers.

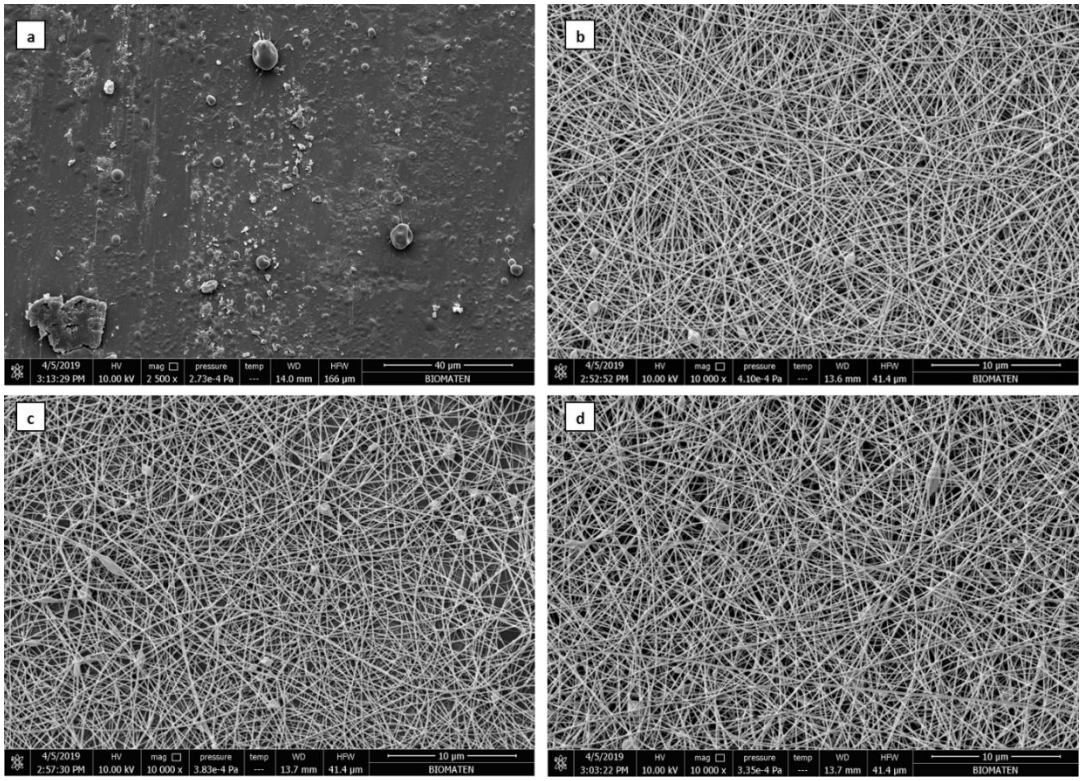

Figure 3.12. SEM images of Ser/Gel (2/1) electrospun scaffolds obtained with different solvents (a) distilled water,(b) 5% acetic acid solution, (c)10% acetic acid solution and (d) 20% acetic acid solution under 20 kV electrical voltage, 2 ml/hr flow rate, and 25 cm distance.

In order to observe the effect of polymer ratios on scaffold microstructure, Ser/Gel polymer mixtures having 0/1, 1/1, 2/1 and 1/2 Ser/Gel ratio with a total polymer concentration of 20 wt% were dissolved in 10 % acetic acid solution and in 20% acetic acid solution; SEM images of the obtained scaffolds are shown in Figure 3.13 and in Figure 3.14, respectively. Electrical voltage, flow rate and distance were set as 20 kV, 2 ml/hr and 25 cm after optimization studies. When the gelatin weight in the polymer mixture was increased bead formation partially diminished in both solvent systems.

The increase in acetic acid concentration from 10% to 20% led to a noticeable decline in the bead formation, especially in the group having 2/1 Ser/Gel ratio. Electrospun fibers composed of only gelatin containing polymer solution (0/1) had larger fibers diameter, but bead-free fiber structure was obtained in 20% acetic acid.

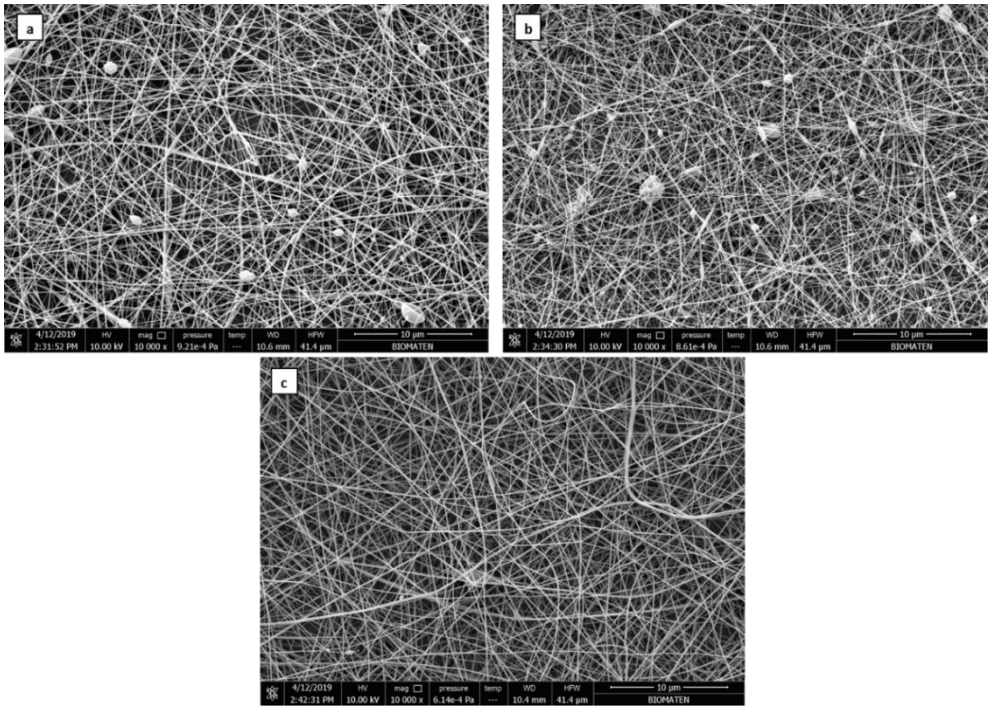

Figure 3.13. SEM images of Ser/Gel (20 wt%) solution dissolved in 10 % acetic acid with (a) 1/1, (b) 2/1 and 1/2 Ser/Gel ratio under 20 kV electrical voltage, 2 ml/hr flow rate, and 25 cm distance.

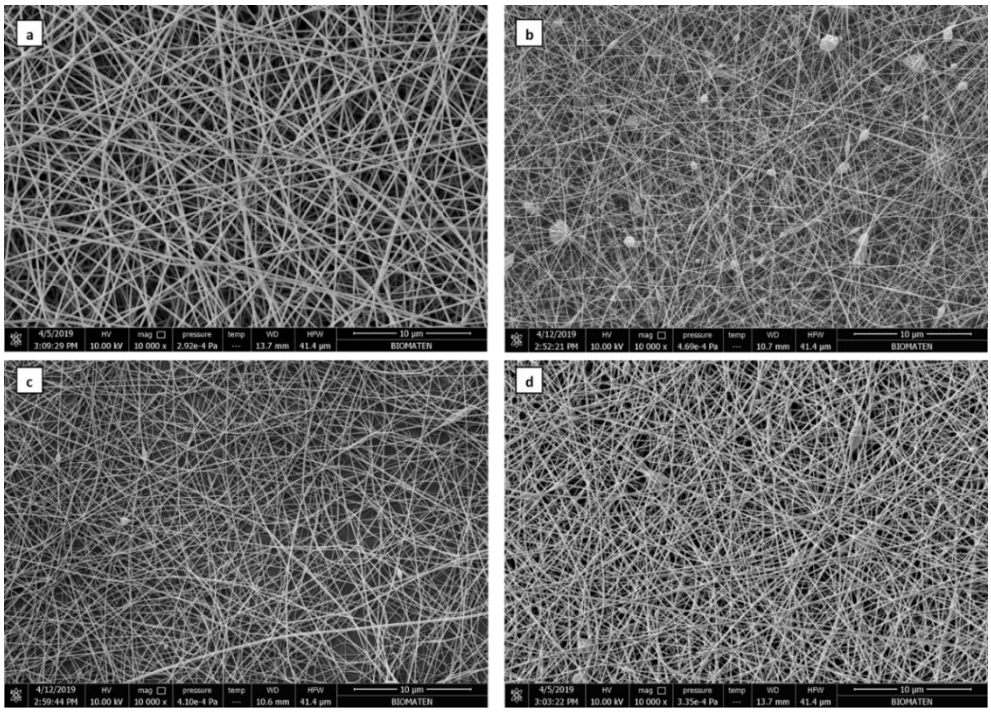

Figure 3.14. SEM images of Ser/Gel (20 wt%) solution dissolved in 20% acetic acid with (a) 0/1, (b) 1/1, (c) 2/1 and (d) 1/2 Ser/Gel ratio under 20 kV electrical voltage, 2 ml/hr flow rate, and 25 cm distance.

Although it appears that the fibers had uniform and smooth surface morphology, particularly the ones having 0/1 and 1/2 Ser/Gel ratio in 20% acetic acid, the yield from the prepared solutions was very low and it was very difficult to collect the fibers from the aluminum coated surface of the collector. Therefore, the experiments with wet spinning method were started for preparation of the scaffolds in in order to collect the fibers easily.

3.6.2. Wet Electrospinning of Sericin/Gelatin Scaffolds

In this study, ethanol was used as an immiscible liquid in wet electrospinning process to collect fibers since it is not dissolving Ser/Gel fibers.

More homogeneous fiber morphology could be acquired with wet electrospinning compared to conventional technique (Yang et al., 2013). Furthermore, it was easy to collect polymer electrospun fibers dropped into a non-solvent liquid on the collector (Atila, Keskin, & Tezcaner, 2015). On the contrary to conventional 2D scaffolds, cell–cell and cell-matrix adhesion is possible with 3-D structures and also, these constructs support cells penetration (Huang et al., 2005).

3.6.2.1. Optimization of Wet Electrospun Sericin/Gelatin Scaffolds with SEM

In order to analyze morphologies of fibers and fiber diameter distributions of the electrospun scaffolds, SEM analyzes were performed. As the fiber conformation were improved with increasing gelatin ratio, wet electrospinning studies were carried out with polymer solutions containing Ser/Gel ratios: 0/1, 1/2, 1/3 and 1/7. However, optimization studies were carried out with scaffold containing 1/2 Ser/Gel ratio.

Solvent Type

During optimization of wet electrospinning, 10% acetic acid, 20% acetic acid and 20% acetic acid solution having 5% DMSO were tested to dissolve both sericin and gelatin polymers. Figure 3.15 shows the fibers formed in (a) 10% acetic acid and (b) 20% acetic acid solution having 5% DMSO. DMSO was added to acetic acid solution to increase dielectric constant of the solvent. One of the important parameters to reduce

bead formation is dielectric constant. While dielectric constant of DMSO is 46.6, that of acetic acid is 6.2. The favorable dielectric constant for electrospinning process is suggested to be higher than 19 and as the dielectric constant of solvent increased, the bead formation decreases (Luo, Stride, & Edirisinghe, 2012). Therefore, DMSO was added to acetic acid solution to increase the dielectric constant of the acetic acid solution.

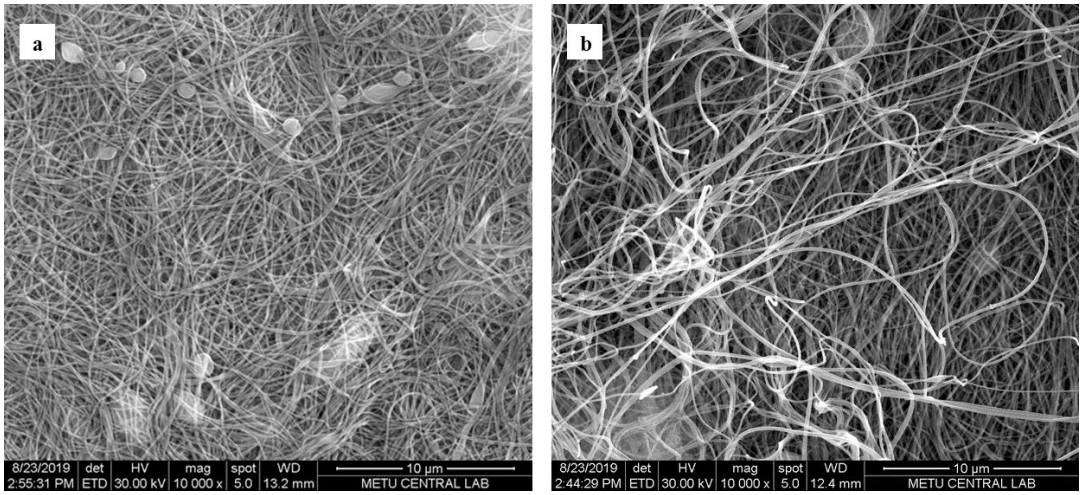

Figure 3.15. SEM images of 1/2 Ser/Gel (20 wt%) solution dissolved in (a) 10% acetic acid and (b) 20% acetic acid solution having 5% DMSO under 20 kV electrical voltage, 2 ml/hr flow rate, and 10 cm distance.

Electrical Voltage

In order to reduce bead formation on the electrospun nanofibers produced from sericin and gelatin, electrical voltage arrangements were done. When the applied electrical voltage increased from 18 kV to 20 kV, bead and irregular aggregate formation decreased on the fibers (Figure 3.16).

In the study to construct chitosan nanofibers, increase in electrical voltage lead to exceeding surface tension of chitosan solution and uniform and homogeneous fibers were obtained (Geng, Kwon, & Jang, 2005).

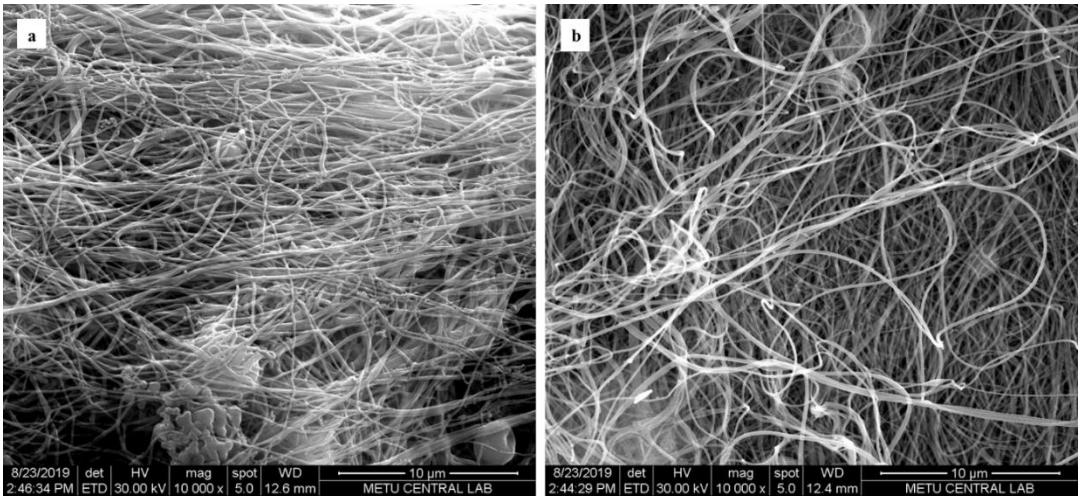

Figure 3.16. SEM images of 1/2 Ser/Gel (20 wt%) solution dissolved in 20% acetic acid solution having 5% DMSO under (a)18 kV and (b)20 kV electrical voltages, 2 ml/hr flow rate, and 10 cm distance.

Flow Rate

Flow rate is the one of the process parameters in electrospinning. Higher flow rates generally prevent charging of the polymer solution and cause thicker and beaded fibers compared to lower flow rates (Li & Wang, 2013).

In this study, different flow rates were examined; 2, 3 and 4 ml/hr. In the scaffold produced with the lowest flow rate, almost bead-free fibers were obtained (Figure 3.17).

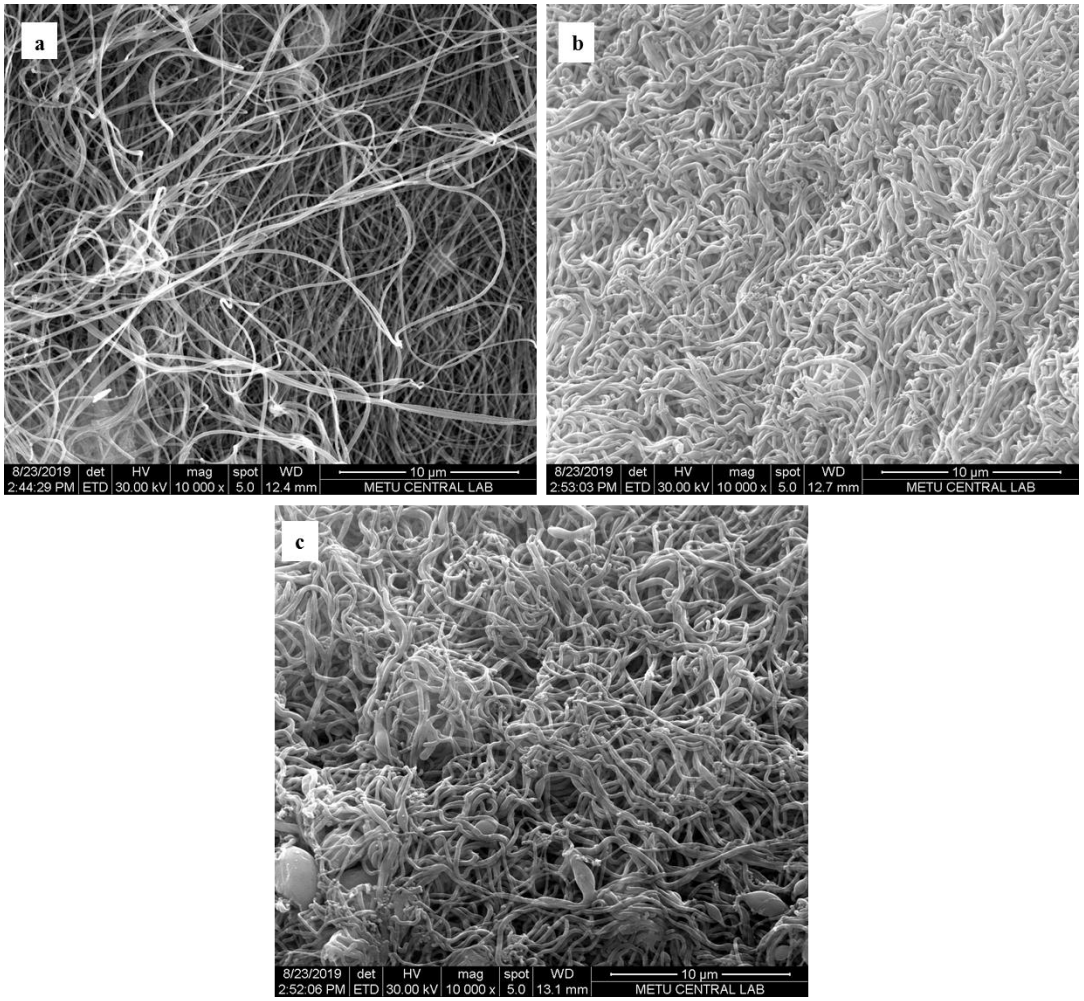

Figure 3.17. SEM images of 1/2 Ser/Gel (20 wt%) solution dissolved in 20% acetic acid solution having 5% DMSO under (a) 2 ml/hr (b) 3 ml/hr and (c) 4 ml/hr flow rates, 20 kV electrical voltage and 10 cm distance.

Total Polymer Concentration

At very low polymer concentrations polymeric particles can be obtained. In this situation, because of the low viscosity and surface tension of polymer solution, electrospraying happens rather than electrospinning (Li & Wang, 2013).

In the case of 10% total polymer concentration, sericin and gelatin containing polymer solution did not form fibers in 20% acetic acid solution having 5% DMSO and under 2 ml/hr flow rate, 20 kV electrical voltage and 10 cm distance (Figure 3.18).

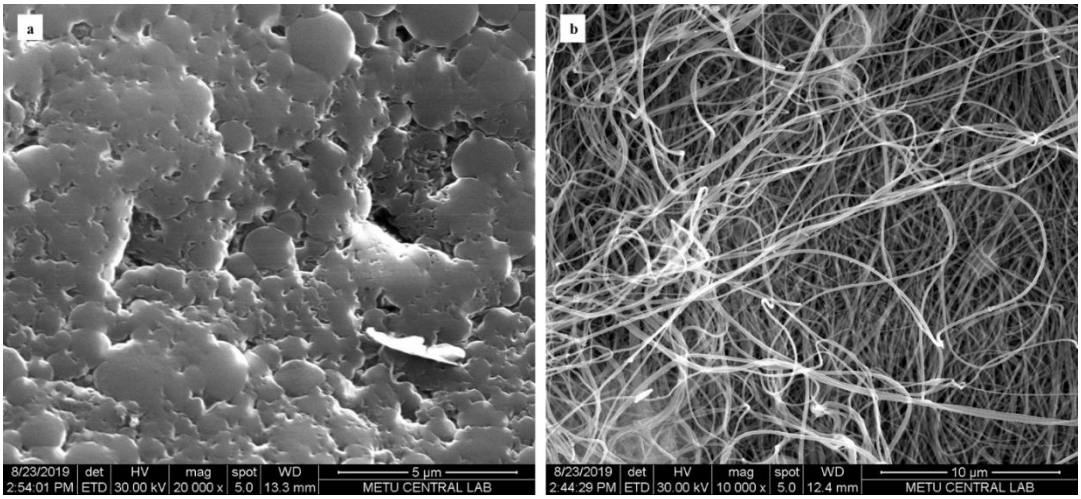

Figure 3.18. SEM images of 1/2 Ser/Gel having (a) 10% and (b) 20 % total polymer concentration dissolved in 20% acetic acid solution having 5% DMSO under 2 ml/hr flow rate, 20 kV electrical voltage and 10 cm distance.

Polymer Composition

SEM images of 0/1 and 1/2 Ser/Gel ratio containing scaffolds are given in Figure 3.19 (All other parameters were kept constant; 20 wt% total polymer concentration, 20 kV electrical voltage, 2 ml/hr flow rate, and 10 cm distance). Sericin addition to the polymer solution did not cause any changes in fiber diameter and bead formation.

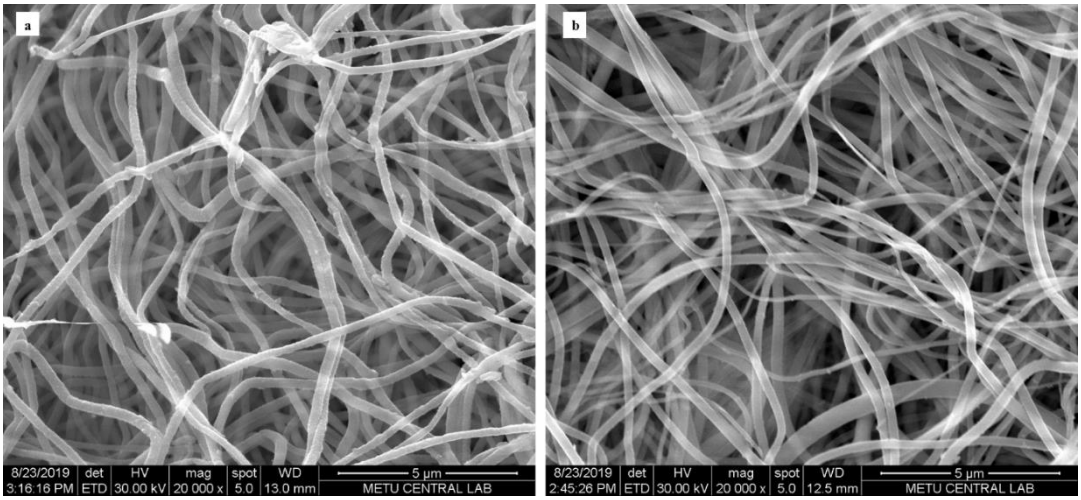

Figure 3.19. SEM images of (a) 0/1 and (b)1/2 Ser/Gel ratio (20 wt %) dissolved in 20% acetic acid solution having 5% DMSO under 2 ml/hr flow rate, 20 kV electrical voltage and 10 cm distance

Crosslinking

Scaffolds were crosslinked with 5% GTA for 1 hr to increase the strength of the fibers. The SEM images of the non-crosslinked and crosslinked scaffolds containing 1/2 and 0/1 Ser/Gel ratio are given in Figure 3.20. Total polymer concentration was 20 wt% and the other parameter were 20 kV electrical voltage, 2 ml/hr flow rate, and 10 cm distance.

After crosslinking, porosity reduced in both of the scaffolds. Fibers containing 1/2 Ser/Gel ratio showed crinkled bundles, however, fibers formed by only gelatin were composed of irregular melting clumps.

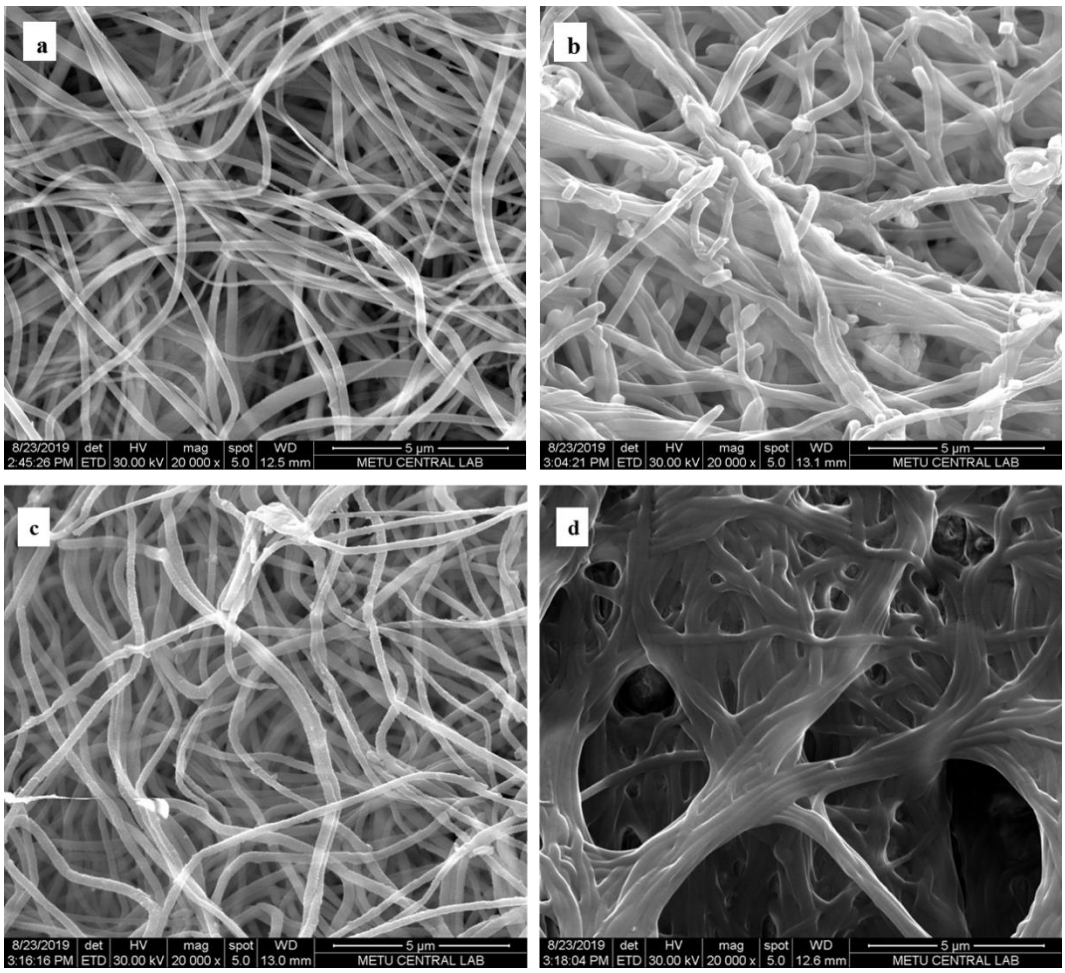

Figure 3.20.SEM image of non-crosslinked (a) and GTA crosslinked (b) scaffolds with 1/2 Ser/Gel ratio (20 wt %) and non-crosslinked (c) and GTA crosslinked (d) scaffolds with 0/1 Ser/Gel ratio (20 wt %) dissolved in 20% acetic acid solution having 5% DMSO under 2 ml/hr flow rate, 20 kV electrical voltage and 10 cm distance

Nanoparticle Loading

The NP loaded scaffold having1/2 Ser/Gel ratio were examined with SEM analysis and NPs are pointed out with red arrows in Figure 3.21. The indicated particles showed similar sizes to that of synthesized PLGA NPs. Parameters were arranged as 20 wt% total polymer concentrations, 2 ml/hr flow rate, 10 cm distance, and electrical voltage 20 kV.

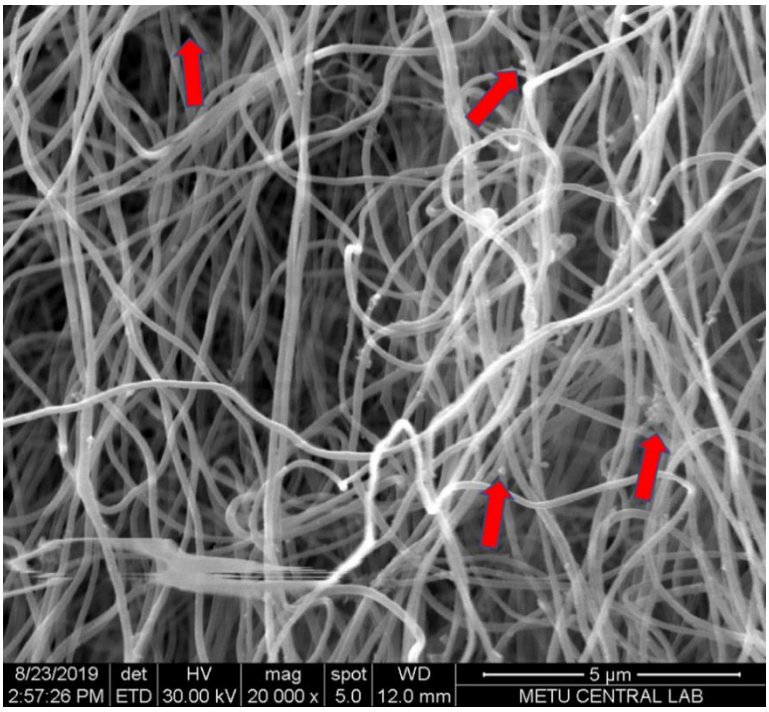

Figure 3.21. SEM images of NP loaded scaffold with 1/2 Ser/Gel ratio (20 wt %) dissolved in 20 % acetic acid solution having 5% DMSO under 2 ml/hr flow rate, 20 kV electrical voltage and 10 cm distance

3.7. Characterization of Wet Electrospun Sericin/Gelatin Scaffolds

3.7.1. Chemical Characterization of Scaffolds

Fourier Transform Infrared Spectroscopy - Attenuated Total Reflectance (FT-IR-ATR) analysis is used to determine the composition of molecules and to detect interactions between molecules (Staroszczyk, Sztuka, Wolska, Wojtasz-Pająk, & Kołodziejska, 2014). In electrospinning studies, FT-IR is applied to specify the effect of crosslinking reactions on electrospun fibers (Chung, Lee, & Choe, 2004).

Crosslinking is a very important process while creating tissue engineering scaffolds using water soluble polymers/proteins. Thus, sericin and gelatin containing scaffolds would easily dissolve in aqueous environment without crosslinking, and this makes them inappropriate for longer term applications.

The characteristic peptide bond occurring in proteins can be observed at absorption bands; 1540 and 1650 cm^{-1} which shows amide II (N-H deformation and C-H stretch) and amide I (C=O stretch), stretching bands, respectively (Chatterji, 1989). Furthermore, C-N stretching and N-H in phase bending can be seen at 1240 cm^{-1} (Sisson et al., 2009). N-H stretching vibration at 3300 cm-1 is seen as distinguishing characteristics of gelatin (Chung et al., 2004).

In this study, amide I, amide II and amide III peaks were determined at 1636, 1530 and 1238 cm^{-1}, respectively, in the FTIR-ATR spectra of the Ser/Gel scaffolds. N-H stretching was observed at 3281 cm^{-1} (Figure 3.22)

It is indicated that absorption band at 1450 cm^{-1} shows the aldimine absorption occurring between aldehyde group (-CHO) of GTA and amine group of gelatin (Nguyen & Lee, 2010). The shift of color of scaffold from white to yellow occurs due to the aldimine linkage (CH=N) formation after GTA crosslinking. In this study, for the crosslinked Gel/Ser scaffold, this band was observed at 1417 cm^{-1}.

Structure of sericin protein is composed of a globular protein having random coil and β-sheets (Kunz et al. 2016). When sericin structure changes from the random coil to the β-sheet, sericin becomes less water soluble (Joseph and Raj 2012). In the study conducted to discover physical properties of sericin membranes cross-linked with dimethylolurea (DMU), the peak at 1516 cm^{-1} was attributed to the β-sheet structure of non-crosslinked sericin (Nagura et al., 2001). In another study, increased intensity of the peak after GTA crosslinking was based on stronger β-sheet formation and this led to more water resistant membrane (Nayak, Talukdar, & Kundu, 2012). In our study, this peak was observed at 1518 cm^{-1} and the peak intensity of the GTA crosslinked scaffold was greater than non-crosslinked one.

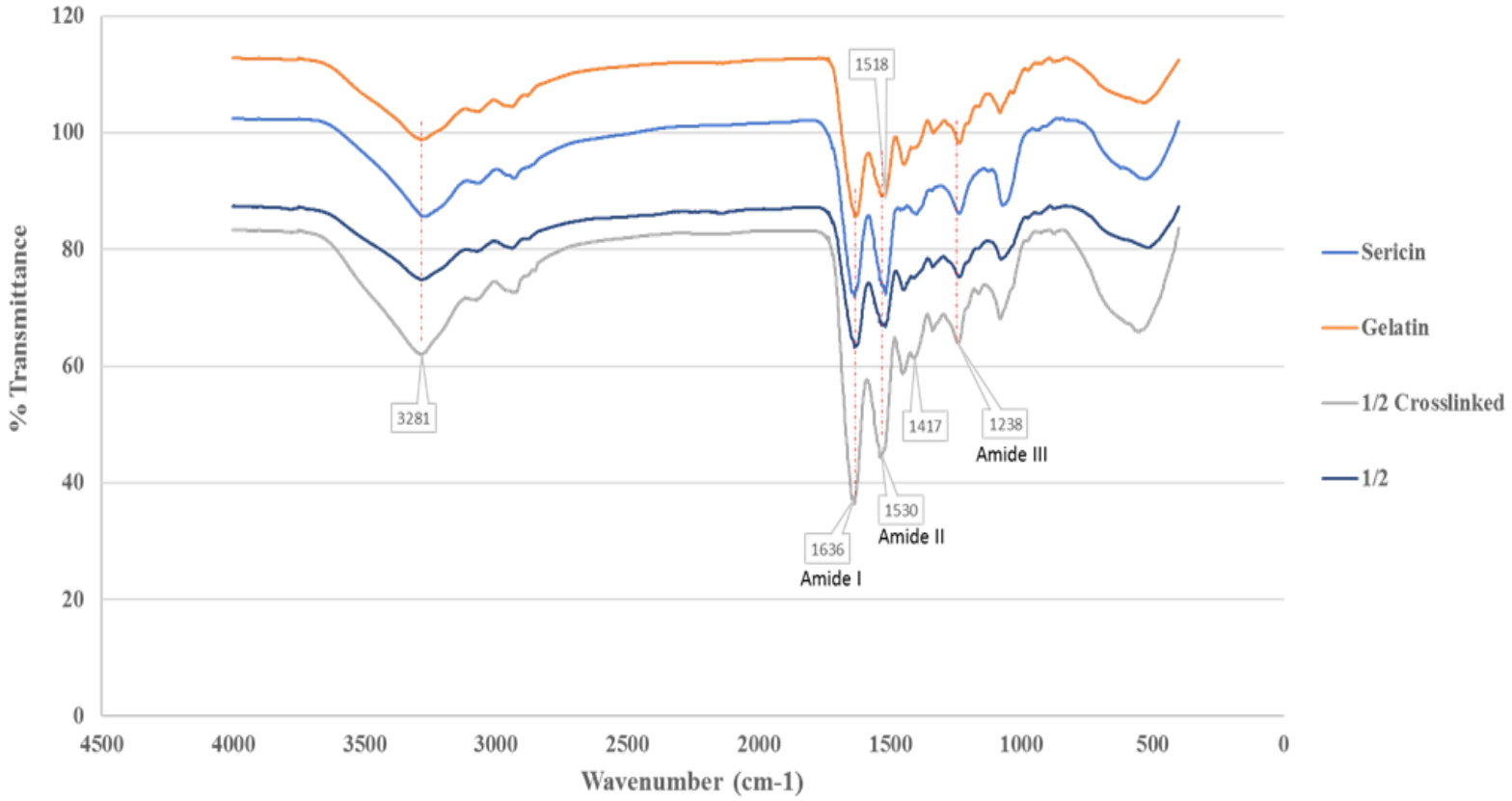

Figure 3.22.FTIR-ATR spectra of sericin and gelatin powders, non-crosslinked scaffold containing 1/2 Ser/Gel ratio and, crosslinked scaffold containing 1/2 Ser/Gel ratio.

3.7.2. *In vitro* Degradation Properties

Degradation studies were performed after crosslinking with GTA since gelatin and sericin are water soluble proteins and non-crosslinked scaffolds were dissolved as soon as they are exposed to PBS (pH 7.4). At the end of the 7-day degradation study, the group having highest amount of gelatin showed greatest weight loss, that is approximately 20% (Figure 3.23). It was seen that during 7 days of PBS incubations, all cross-linked Ser/Gel scaffolds retained their structural stability. Degree of weight loss elevated when the amount of gelatin increased.

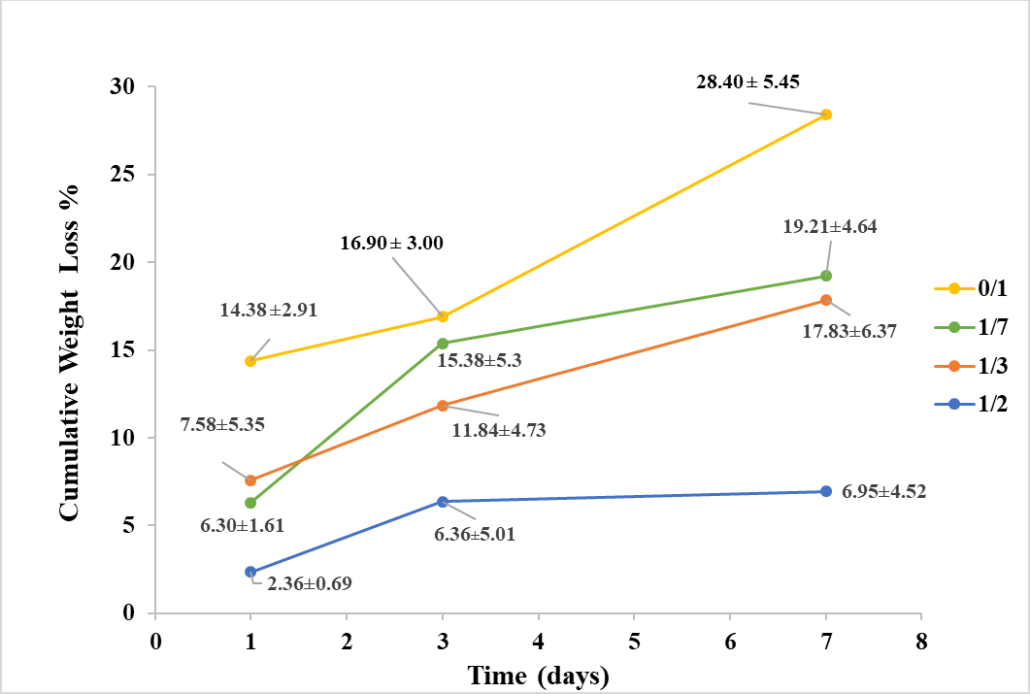

Figure 3.23. Degradation studies of corsslinked scaffolds having different Ser/Gel ratio. The data are represented as mean ± Std. (n = 3).

3.7.3. Water Absorption

The degree of Ser/Gel scaffold swelling after immersion in PBS was shown in Figure 3.24. The highest swelling degree was detected in 1/7 and 0/1 Ser/Gel ratio containing groups, while the minimum was observed in the case of 1/2 Ser/Gel scaffolds. The swelling degree slowly increased over time and rise in sericin amount in the scaffold led to less swelling. Nevertheless, the scaffold showing the lowest swelling degree on

1st day swelled extensively in water and hold water nearly 5 times of its weight. However, the statistical analysis conducted by two-way ANOVA with Tukey's comparison test (p=0.05) showed that water the retention degree of all scaffolds was not significantly different.

Similarly, it was claimed that increase in sericin concentration decreased swelling of sericin/gelatin films that were prepared by blending sericin and gelatin proteins in the presence of glutaraldehyde as cross-linker (Mandal et al., 2009).

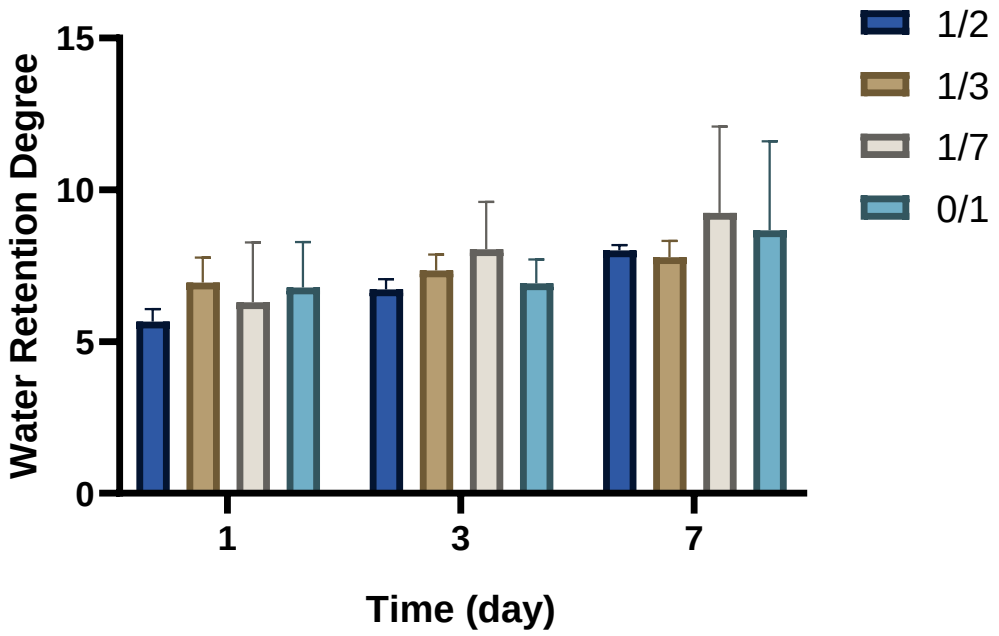

Figure 3.24. Water absoption studies of scaffolds having 1/2, 1/3 and 1/7 Ser/Gel ratio in PBS (pH=7,4). The data are represented as the mean ± Std. (n = 3).

3.8. Heparin Release Results from Scaffolds

The release profiles of the heparin from PLGA NPs loaded scaffolds having 0/1 and 1/2 Ser/Gel ratio are given in Figure 3.25. The initial weight ratio of nanoparticles to polymer was 20% (w/w), that is, 100 mg of NP was added to the solution containing 400 mg of polymer. Since there was approximately 3 mg (540 IU) of heparin was present in 100 mg of NPs, 3.375 IU/ml HP was calculated in 5 mg of scaffold.

Nearly 65% of HP was released from scaffold having only gelatin and approximately 40% HP was released from the scaffold having 1/2 Ser/Gel ratio at the end of the 7th day. The reason of this different release profiles from different scaffold may be rapid degradation of only gelatin containing scaffold compared the other group. NPs in 0/1 Ser/Gel containing group interact with aqueous environment more because of its rapid degradation compared to 1/2 Ser/Gel scaffold.

The release from NPs was much higher than it was expected (Figure 3.9). Loading the NPs to the scaffold decelerated the release of HP from the scaffolds.

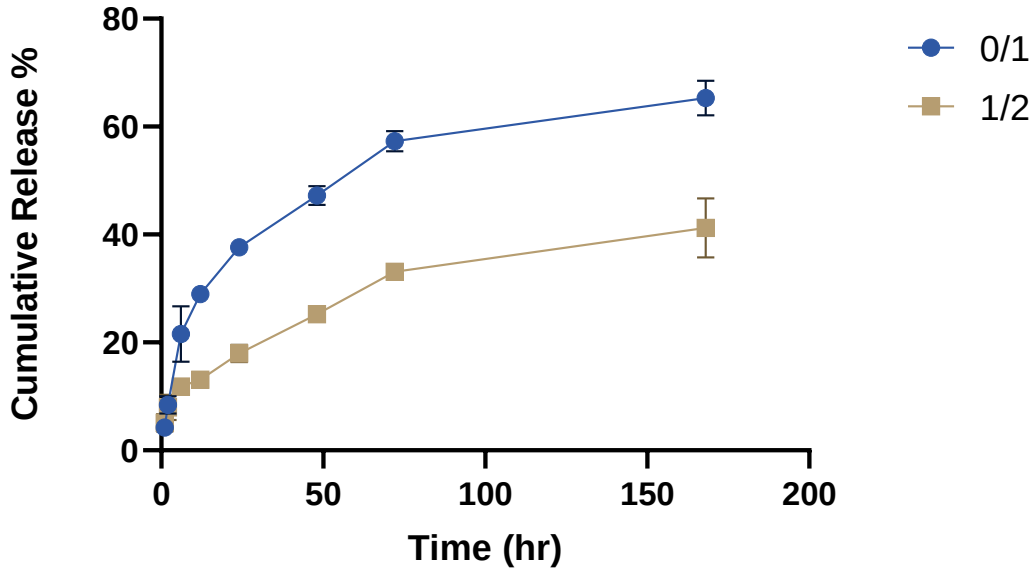

Figure 3.25. Cumulative release of heparin from NP-loaded 1/2 and 0/1 Ser/Gel ratio having scaffolds. The data are represented as the mean ± Std. (n=3)

3.9. Cell Culture Studies for Scaffolds

3.9.1. Cell Attachment and Proliferation Analysis

Alamar Blue cell viability assay was performed to investigate the attachment and proliferation of cells on electrospun scaffolds. L929 cells were seeded on scaffolds at concentration of 1x10^4 cells/scaffold and the results were taken at 1st, 3rd and 5th days.

In Figure 3.26, cell viability of L929 cells seeded on scaffolds are illustrated. For all groups, NP containing scaffolds increased the cell proliferation day by day and reached the maximum proliferation of cells at 5th day. All NP containing scaffolds showed similar pattern in terms of cell proliferation; nearly 80% cell proliferation rate for 5th day. However, cells seeded on scaffolds without NPs showed less cell viability. Besides, scaffolds having 1/2 and 1/7 Ser/Gel ratio had the lowest cell viability at 5th day. Cells seeded on scaffolds showed statistically lower cell viability than positive control (TCPS) as determined by two-way ANOVA with Tukey's comparison test ($P<0.0001$).

Cells on the scaffolds did not proliferate as much as the cells seeded on TCPS. The reason for could be due to lower attachment of cell on scaffolds rather than TCPS, but they approached similar cell proliferation percent with TCPS in 5 days.

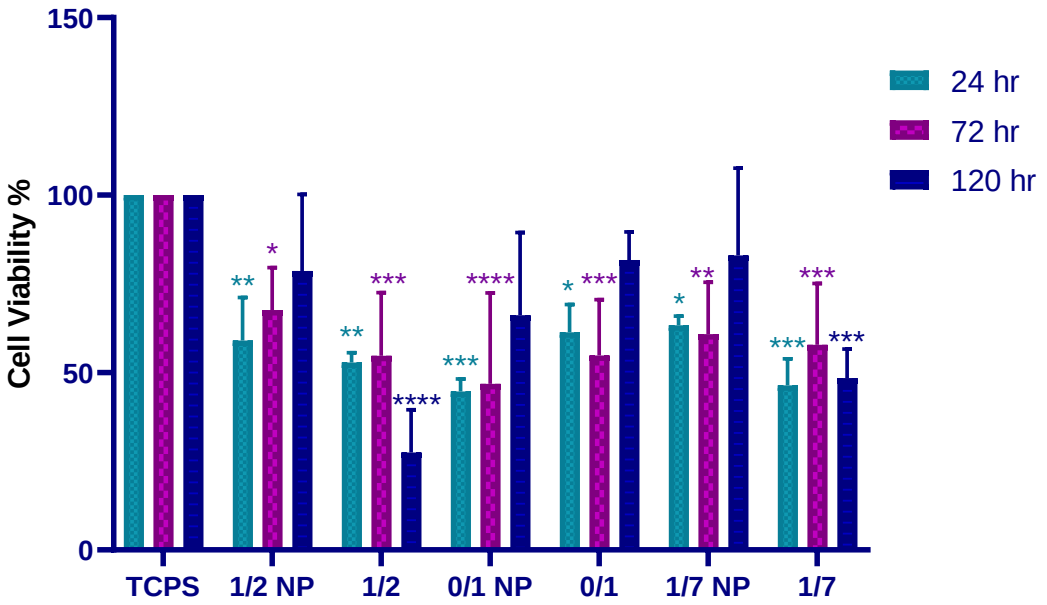

*Figure 3.26.Relative viability of L-929 cells seeded on NP loaded and unloaded scaffolds containing different Ser/Gel ratio at 1st, 3rd and 5th days of incubation. Viability on TCPS was accepted as 100%. The data are represented as the mean ± Std. (n = 3) and * shows significant difference between groups.*

The reason of high proliferation on NP containing scaffolds may be controlled delivery of HP from NPs since HP stimulates proliferation of fibroblast cells (Yamashita et al., 1992).

3.9.2. Cell Morphology Analysis

SEM analysis were performed after cell fixation protocol. Cell morphology of cells seeded on the 0/1 and 1/2 Ser/Gel ratio having scaffolds at 3rd day of incubation is shown in Figure 3.27. SEM images showed that the fibroblasts attached to the surface by filopodia on 0/1 scaffolds and cells covering the surface can be seen on 1/2 scaffolds. There was no cell detected on the other scaffolds due to low cell seeding density.

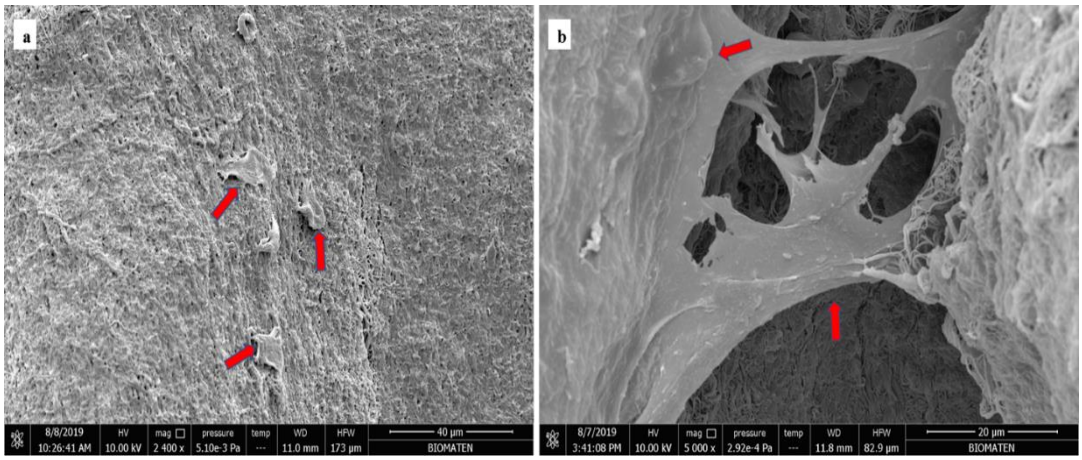

Figure 3.27. SEM images of cells seeded on (a) 0/1 and (b) 1/2 Ser/Gel ratio containing scaffolds at 3th day of incubation.

CHAPTER 4

CONCLUSION

Skin damages should be repaired and regenerated as soon as possible, since skin protects entire body against pathogens/microbes and maintains the homeostasis in the body. In order to get skin tissue engineering constructs that enable rapid and effective healing, electrospun sericin/gelatin composite nanofibers were produced. Ser/Gel electrospun fibers incorporating HP-loaded NPs were produced successfully and investigated with *in vitro* studies as scaffolds for skin tissue engineering. In this study, HP was encapsulated in PLGA NPs. These synthesized NPs were mixed with Ser/Gel polymer solutions having various weight ratios and electrospun with polymer solution for the first time in literature. Performed GTA crosslinking for sericin/gelatin composite material considerably enhanced durability of the developed scaffolds according to degradation studies. The scaffold having 1⁄2 Ser/Gel proportion was preferred due to its proper fiber morphology and lowest degradation degree.

It was observed that NPs have no cytotoxic effects on L929 cells. Cells that were grown on HP-loaded NP containing scaffolds also showed higher cell viability compared to the ones exposed to only scaffolds. Numerical increase in cell viability on HP-loaded NP containing scaffolds compared to un-loaded scaffolds suggests that these constructs can be used safely for skin tissue engineering purposes.

As future study, in order to examine if heparin activity has changed after released from nanoparticles or scaffolds having NPs, HP activity assay can be performed. Convenience of scaffolds for cell penetration can be analyzed with porosity measurements. Cell migration through scaffolds can be determined by staining cells with DAPI and by examining the results with confocal laser scanning microscopy.

Furthermore, in order to observe wound healing/skin regeneration potency of the produced materials, further research is needed with *in vivo* experiments.

REFERENCES

Adnan Haidera, Sajjad Haiderb, & Inn-Kyu Kanga. (2015). A comprehensive review summarizing the effect of electrospinning parameters and potential applications of nanofibers in biomedical and biotechnology. *Arabian Journal of Chemistry*.

Agrahari, V., Agrahari, V., Meng, J., & Mitra, A. K. (2017). Electrospun Nanofibers in Drug Delivery. In *Emerging Nanotechnologies for Diagnostics, Drug Delivery and Medical Devices*. https://doi.org/10.1016/B978-0-323-42978-8.00009-7

Ahsan, F., Ansari, T. M., Usmani, S., & Bagga, P. (2018). An Insight on Silk Protein Sericin: From Processing to Biomedical Application. *Drug Research*. https://doi.org/10.1055/s-0043-121464

Akturk, O., Tezcaner, A., Bilgili, H., Deveci, M. S., Gecit, M. R., Keskin, D., & Ioeng, J. B. I. B. (2011). Evaluation of sericin / collagen membranes as prospective wound dressing biomaterial. *JBIOSC*, *112*(3), 279–288. https://doi.org/10.1016/j.jbiosc.2011.05.014

American Society for Surgery of the Hand. (2014). Burns - Symptoms and Treatment - The Hand Society.

Atila, D., Keskin, D., & Tezcaner, A. (2015). Cellulose acetate based 3-dimensional electrospun scaffolds for skin tissue engineering applications. *Carbohydrate Polymers*, *133*, 251–261. https://doi.org/10.1016/j.carbpol.2015.06.109

Balusamy, B., Senthamizhan, A., & Uyar, T. (2017). Electrospun nanofibrous materials for wound healing applications. *Electrospun Materials for Tissue Engineering and Biomedical Applications*, 147–177. https://doi.org/10.1016/B978-0-08-101022-8.00012-0

Bhardwaj, N., & Kundu, S. C. (2010). Electrospinning: A fascinating fiber fabrication technique. *Biotechnology Advances*, *28*(3), 325–347. https://doi.org/10.1016/j.biotechadv.2010.01.004

Boateng, J. S., Matthews, K. H., Stevens, H. N. E., & Eccleston, G. M. (2008). Wound Healing Dressings and Drug Delivery Systems: A Review. *Journal of Pharmaceutical Sciences*, *97*(8), 2892–2923. https://doi.org/10.1002/jps.21210

BOGNITZKI M., CZADO W., FRESE T., SCHAPER A., HELLWIG M., S., & M. (2001). Nanostructured fibers via electrospinning. *Advanced Materials (Deerfield Beach, Fla.)*.

Carroll, L. a, & Koch, R. J. (2003). Heparin stimulates production of bFGF and TGF-beta 1 by human normal, keloid, and fetal dermal fibroblasts. *Medical Science Monitor : International Medical Journal of Experimental and Clinical Research*.

Chatterji, P. R. (1989). Gelatin with hydrophilic/hydrophobic grafts and glutaraldehyde crosslinks. *Journal of Applied Polymer Science*, *37*(8), 2203–2212. https://doi.org/10.1002/app.1989.070370812

Chen, G., & Wen, J. (2018). Poly(lactic-co-glycolic acid) based double emulsion nanoparticle as a carrier system to deliver glutathione sublingually. *Journal of Biomedicine*, *3*, 50–59. https://doi.org/10.7150/jbm.27148

Chen, S., Liu, B., Carlson, M. A., Gombart, A. F., Reilly, D. A., & Xie, J. (2017). Recent advances in electrospun nanofibers for wound healing. *Nanomedicine*, *12*(11), 1335–1352. https://doi.org/10.2217/nnm-2017-0017

Chung, C., Lee, M., & Choe, E. K. (2004). Characterization of cotton fabric scouring by FT-IR ATR spectroscopy. *Carbohydrate Polymers*, *58*(4), 417–420. https://doi.org/10.1016/J.CARBPOL.2004.08.005

Coulson-Thomas, V., & Gesteira, T. (2016). Dimethylmethylene Blue Assay (DMMB). *BIO-PROTOCOL*. https://doi.org/10.21769/bioprotoc.1236

Dabiri, G., Damstetter, E., & Phillips, T. (2016). Choosing a Wound Dressing Based on Common Wound Characteristics. *Advances in Wound Care*. https://doi.org/10.1089/wound.2014.0586

Dash Bieaja C. ; Hsia Henry C. (2019). *Biomaterials for Skin Repair and Regeneration - Google Kitaplar* (Elena Garcia-Gareta, Ed.). United States: Matthew Deans.

De Vrieze, S., Van Camp, T., Nelvig, A., Hagström, B., Westbroek, P., & De Clerck, K. (2009). The effect of temperature and humidity on electrospinning. *Journal of Materials Science*. https://doi.org/10.1007/s10853-008-3010-6

Deitzel, J. M., Kleinmeyer, J., Harris, D., & Beck Tan, N. C. (2001). The effect of processing variables on the morphology of electrospun nanofibers and textiles. *Polymer*. https://doi.org/10.1016/S0032-3861(00)00250-0

Deng, C. M., He, L. Z., Zhao, M., Yang, D., & Liu, Y. (2007). Biological properties of the chitosan-gelatin sponge wound dressing. *Carbohydrate Polymers*. https://doi.org/10.1016/j.carbpol.2007.01.014

Dhivya, S., Padma, V. V., & Santhini, E. (2015). Wound dressings - A review. *BioMedicine (Netherlands)*. https://doi.org/10.7603/s40681-015-0022-9

Eaton, P., Quaresma, P., Soares, C., Neves, C., de Almeida, M. P., Pereira, E., & West, P. (2017). A direct comparison of experimental methods to measure dimensions of synthetic nanoparticles. *Ultramicroscopy*, *182*, 179–190. https://doi.org/10.1016/j.ultramic.2017.07.001

Ersel, M., Uyanikgil, Y., Karbek Akarca, F., Ozcete, E., Altunci, Y. A., Karabey, F., … Oyku Cetin, E. (2016). Effects of Silk Sericin on Incision Wound Healing in a Dorsal Skin Flap Wound Healing Rat Model. *Medical Science Monitor*, *22*, 1064–1078. https://doi.org/10.12659/MSM.897981

Freiberg, S., & Zhu, X. X. (2004). Polymer microspheres for controlled drug release. *International Journal of Pharmaceutics*. https://doi.org/10.1016/j.ijpharm.2004.04.013

Geng, X., Kwon, O. H., & Jang, J. (2005). Electrospinning of chitosan dissolved in concentrated acetic acid solution. *Biomaterials*, *26*(27), 5427–5432. https://doi.org/10.1016/j.biomaterials.2005.01.066

Gentile, P., Chiono, V., Carmagnola, I., & Hatton, P. V. (2014). An overview of poly(lactic-co-glycolic) Acid (PLGA)-based biomaterials for bone tissue engineering. *International Journal of Molecular Sciences*, *15*(3), 3640–3659. https://doi.org/10.3390/ijms15033640

Goldsmith, L. A. (1991). *Physiology, biochemistry, and molecular biology of the skin*. Oxford University Press.

Gonzalez, A. C. de O., Costa, T. F., Andrade, Z. de A., & Medrado, A. R. A. P. (2016). Wound healing-A literature review. *Anais Brasileiros de Dermatologia*, *91*(5), 614–620.

Gupta, B. S., & Moghe, A. K. (2013). Nanofiber structures for medical biotextiles. In *Biotextiles As Medical Implants*. https://doi.org/10.1533/9780857095602.1.48

Gupta, V., & Trivedi, P. (2018). In vitro and in vivo characterization of pharmaceutical topical nanocarriers containing anticancer drugs for skin cancer treatment. In *Lipid Nanocarriers for Drug Targeting*. https://doi.org/10.1016/b978-0-12-813687-4.00015-3

H. Panda. (2009). Nanotechnology Handbook: Polymer Nanofibers Processing Business Ideas You ... - H. Panda - Google Kitaplar.

Haider, A., Haider, S., & Kang, I. K. (2018). A comprehensive review summarizing the effect of electrospinning parameters and potential applications of nanofibers in biomedical and biotechnology. *Arabian Journal of Chemistry*. https://doi.org/10.1016/j.arabjc.2015.11.015

Hoffart, V., Ubrich, N., Simonin, C., Babak, V., Vigneron, C., Hoffman, M., … Maincent, P. (2002). Low molecular weight heparin-loaded polymeric nanoparticles: Formulation, characterization, and release characteristics. *Drug Development and Industrial Pharmacy*, *28*(9), 1091–1099. https://doi.org/10.1081/DDC-120014576

Hoffman Matthew. (2014). The Skin (Human Anatomy): Picture, Definition, Function, and Skin Conditions.

Huang, Y., Onyeri, S., Siewe, M., Moshfeghian, A., & Madihally, S. V. (2005). In vitro characterization of chitosan-gelatin scaffolds for tissue engineering. *Biomaterials*, *26*(36), 7616–7627. https://doi.org/10.1016/j.biomaterials.2005.05.036

Hussein, A. S., Fakhru'l-Razi, A., & Abdullah, N. (2013). Preparation and Characterization of Poly (D,L-Lactide-co-Glycolide) (PLGA) Nanoparticles Loaded with Linamarin for Controlled Drug Release. *International Journal of Polymer Analysis and Characterization*, *18*(6), 414–422. https://doi.org/10.1080/1023666X.2013.786864

Iqbal, M., Zafar, N., Fessi, H., & Elaissari, A. (2015). Double emulsion solvent evaporation techniques used for drug encapsulation. *International Journal of Pharmaceutics*. https://doi.org/10.1016/j.ijpharm.2015.10.057

Jang, H. J., Kim, Y. M., Yoo, B. Y., & Seo, Y. K. (2018). Wound-healing effects of human dermal components with gelatin dressing. *Journal of Biomaterials Applications*. https://doi.org/10.1177/0885328217741758

Jiao, Y., Ubrich, N., Marchand-Arvier, M., Vigneron, C., Hoffman, M., Lecompte, T., & Maincent, P. (2002). In vitro and in vivo evaluation of oral heparin-loaded polymeric nanoparticles in rabbits. *Circulation*, *105*(2), 230–235. https://doi.org/10.1161/hc0202.101988

Jones, V., E Grey, J., & G Harding, K. (2006). ABC of wound healing. Wound dressings. *British Medical Journal*. https://doi.org/10.1136/bmj.332.7544.777

Jusman, Y., Ng, S. C., & Abu Osman, N. A. (2014). Investigation of CPD and HMDS sample preparation techniques for cervical cells in developing computer-aided screening system based on FE-SEM/EDX. *Scientific World Journal*, *2014*. https://doi.org/10.1155/2014/289817

Khurshid, C., & Pye, D. A. (2018). Isolation and Composition Analysis of Bioactive Glycosaminoglycans from Whelk. *Marine Drugs*, *16*(5). https://doi.org/10.3390/md16050171

Kim, D. H., & Martin, D. C. (2006). Sustained release of dexamethasone from hydrophilic matrices using PLGA nanoparticles for neural drug delivery. *Biomaterials*, *27*(15), 3031–3037. https://doi.org/10.1016/j.biomaterials.2005.12.021

Kny, E., Ghosal, K., & Thomas, S. (2018). *Electrospinning: Frm Basic Research to Commercialization* (Vol. 7). Royal Society of Chemistry.

Krishnaswamy, K., & Orsat, V. (2017). Sustainable Delivery Systems Through Green Nanotechnology. In *Nano- and Microscale Drug Delivery Systems: Design and Fabrication*. https://doi.org/10.1016/B978-0-323-52727-9.00002-9

Kundu, S. C., Dash, B. C., Dash, R., & Kaplan, D. L. (2008). Natural protective glue protein, sericin bioengineered by silkworms: Potential for biomedical and biotechnological applications. *Progress in Polymer Science (Oxford)*. https://doi.org/10.1016/j.progpolymsci.2008.08.002

Laurent, A., Mistretta, F., Bottigioli, D., Dahel, K., Goujon, C., Nicolas, J. F., … Laurent, P. E. (2007). Echographic measurement of skin thickness in adults by high frequency ultrasound to assess the appropriate microneedle length for intradermal delivery of vaccines. *Vaccine*, *25*(34), 6423–6430. https://doi.org/10.1016/J.VACCINE.2007.05.046

Li, Z., & Wang, C. (2013). *One dimensional Nanostructures Electrospinning Technique and Unique Nanofibers*. https://doi.org/10.1007/978-3-642-36427-3

Lin, B., Fabbi, M., & Driver, V. R. (2011). The Role of Heparin in Wound Healing. *Advances in Wound Care*, *2*. https://doi.org/10.1089/9781934854280.273

Liu, Y., Cai, S., Shu, X. Z., Shelby, J., & Prestwich, G. D. (2007). Release of basic fibroblast growth factor from a crosslinked glycosaminoglycan hydrogel promotes wound healing. *Wound Repair and Regeneration*. https://doi.org/10.1111/j.1524-475X.2007.00211.x

Lu, G. W., & Gao, P. (2009). Emulsions and Microemulsions for Topical and Transdermal Drug Delivery. In *Handbook of Non-Invasive Drug Delivery Systems*. https://doi.org/10.1016/b978-0-8155-2025-2.10003-4

Luo, C. J., Stride, E., & Edirisinghe, M. (2012). Mapping the influence of solubility and dielectric constant on electrospinning polycaprolactone solutions. *Macromolecules*, *45*(11), 4669–4680. https://doi.org/10.1021/ma300656u

Makadia, H. K., & Siegel, S. J. (2011). Poly Lactic-co-Glycolic Acid (PLGA) as Biodegradable Controlled Drug Delivery Carrier. *Polymers*. https://doi.org/10.3390/polym3031377

Mandal, B. B., Priya, A. S., & Kundu, S. C. (2009). Novel silk sericin / gelatin 3-D scaffolds and 2-D films : Fabrication and characterization for potential tissue engineering applications. *Acta Biomaterialia*, *5*(8), 3007–3020. https://doi.org/10.1016/j.actbio.2009.03.026

Martins, A. F., de Oliveira, D. M., Pereira, A. G. B., Rubira, A. F., & Muniz, E. C. (2012). Chitosan/TPP microparticles obtained by microemulsion method applied in controlled release of heparin. *International Journal of Biological Macromolecules*, *51*(5), 1127–1133. https://doi.org/10.1016/j.ijbiomac.2012.08.032

Maynard John. (2015). How Wounds Heal: The 4 Main Phases of Wound Healing | Shield HealthCare.

Megelski, S., Stephens, J. S., Bruce Chase, D., & Rabolt, J. F. (2002). Micro- and nanostructured surface morphology on electrospun polymer fibers. *Macromolecules*, *35*(22), 8456–8466. https://doi.org/10.1021/ma020444a

Metcalfe, A. D., & Ferguson, M. W. . (2007). Tissue engineering of replacement skin: the crossroads of biomaterials, wound healing, embryonic development, stem cells and regeneration. *Journal of The Royal Society Interface*, *4*(14), 413–437. https://doi.org/10.1098/rsif.2006.0179

Muthu, M. (2010). Nanoparticles based on PLGA and its co-polymer: An overview. *Asian Journal of Pharmaceutics*. https://doi.org/10.4103/0973-8398.59948

Nagura, M., Ohnishi, R., Gitoh, Y., & Ohkoshi, Y. (2001). Structures and physical properties of cross-linked sericin membranes. *Journal of Sericultural Science of Japan*, *70*(2), 149–153.

Nayak, S., Talukdar, S., & Kundu, S. C. (2012). *Potential of 2D crosslinked sericin membranes with improved biostability for skin tissue engineering*. 783–794. https://doi.org/10.1007/s00441-011-1269-4

Nguyen, T.-H., & Lee, B.-T. (2010). Fabrication and characterization of cross-linked gelatin electro-spun nano-fibers. *Journal of Biomedical Science and Engineering*, *03*(12), 1117–1124. https://doi.org/10.4236/jbise.2010.312145

Nurunnabi, M., Revuri, V., Huh, K. M., & Lee, Y. kyu. (2017). Polysaccharide based nano/microformulation: An effective and versatile oral drug delivery system. In *Nanostructures for Oral Medicine*. https://doi.org/10.1016/B978-0-323-47720-8.00015-8

Olczyk, P., Mencner, Ł., & Komosinska-Vassev, K. (2015). Diverse Roles of Heparan Sulfate and Heparin in Wound Repair. *BioMed Research International*, *2015*. https://doi.org/10.1155/2015/549417

Ovington, L. G. (2007). Advances in wound dressings. *Clinics in Dermatology*. https://doi.org/10.1016/j.clindermatol.2006.09.003

Oyarzun-Ampuero, F. A., Brea, J., Loza, M. I., Torres, D., & Alonso, M. J. (2009). Chitosan-hyaluronic acid nanoparticles loaded with heparin for the treatment of asthma. *International Journal of Pharmaceutics*, *381*(2), 122–129. https://doi.org/10.1016/j.ijpharm.2009.04.009

Pankaew, P., White, P., & Naemchanthara, K. (2015). *A Study of the Preparation of Silk Sericin / Chitosan Composite Film for Future A Study of the Preparation of Silk Sericin / Chitosan Composite Film for Future Wound Dressing Applications*. (October). https://doi.org/10.4028/www.scientific.net/AMM.804.179

Pate, K., & Safier, P. (2016). Chemical metrology methods for CMP quality. *Advances in Chemical Mechanical Planarization (CMP)*, 1–325. https://doi.org/10.1016/B978-0-08-100165-3.00012-7

Pei, Y., Ye, D., Zhao, Q., Wang, X., Zhang, C., Huang, W., … Zhang, L. (2015). cellulose / gelatin sponges constructed directly. *Journal of Materials Chemistry B*. https://doi.org/10.1039/C5TB00477B

Pillay, V., Dott, C., Choonara, Y. E., Tyagi, C., Tomar, L., Kumar, P., … Ndesendo, V. M. K. (2013). A review of the effect of processing variables on the fabrication of electrospun nanofibers for drug delivery applications. *Journal of Nanomaterials*, *2013*. https://doi.org/10.1155/2013/789289

Qi, C., Xu, L., Deng, Y., Wang, G., Wang, Z., & Wang, L. (2018). Sericin hydrogels promote skin wound healing with effective regeneration of hair follicles and sebaceous glands after complete loss of epidermis and dermis. *Biomaterials Science*. https://doi.org/10.1039/c8bm00934a

Radivojša, M., Grabnar, I., & Grabnar, P. A. (2013). Thermoreversible in situ gelling poloxamer-based systems with chitosan nanocomplexes for prolonged subcutaneous delivery of heparin: Design and in vitro evaluation. *European Journal of Pharmaceutical Sciences*. https://doi.org/10.1016/j.ejps.2013.03.002

Raja Nhari, R. M. H., Che Man, Y., Ismail, A., & Anuar, N. (2011). Chemical and functional properties of bovine and porcine skin gelatin. *International Food Research Journal*, *817*(June), 813–817.

Rangari, A. T. (2015). Polymeric Nanoparticles Based Topical Drug Delivery: An Overview. *Asian Journal of Biomedical and Pharmaceutical Sciences*. https://doi.org/10.15272/ajbps.v5i47.718

Reinke, J. M., & Sorg, H. (2012). Wound repair and regeneration. *European Surgical Research*. https://doi.org/10.1159/000339613

Rosenberg, R. D., & Lam, L. (2006). Correlation between structure and function of heparin. *Proceedings of the National Academy of Sciences*. https://doi.org/10.1073/pnas.76.3.1218

Saghazadeh, S., Rinoldi, C., Schot, M., Kashaf, S. S., Sharifi, F., Jalilian, E., … Khademhosseini, A. (2018). Drug delivery systems and materials for wound healing applications. *Advanced Drug Delivery Reviews*, *127*, 138–166. https://doi.org/10.1016/j.addr.2018.04.008

Saliba, M. J. (2001). Heparin in the treatment of burns: A review. *Burns*, *27*(4), 349–358. https://doi.org/10.1016/S0305-4179(00)00130-3

Sapru, S., Das, S., Mandal, M., Ghosh, A. K., & Kundu, S. C. (2018). Acta Biomaterialia Prospects of nonmulberry silk protein sericin-based nanofibrous matrices for wound healing – In vitro and in vivo investigations. *Acta Biomaterialia*, *78*, 137–150. https://doi.org/10.1016/j.actbio.2018.07.047

Sarabahi, S. (2012). Recent advances in topical wound care. *Indian Journal of Plastic Surgery*. https://doi.org/10.4103/0970-0358.101321

Sill, T. J., & von Recum, H. A. (2008). Electrospinning: Applications in drug delivery and tissue engineering. *Biomaterials*. https://doi.org/10.1016/j.biomaterials.2008.01.011

Singh Gurpreet, Kaur Tanurajvir, Kaur Ravinder, K. A. (2014). Recent biomedical applications and patents on biodegradable polymer-PLGA. *International Journal of Pharmacology and Pharmaceutical Sciences [ISSN:2394-613X]*, *1*(2), 30–42. https://doi.org/http://citeseerx.ist.psu.edu/viewdoc/download?doi=10.1.1.679.2373&rep=rep1&type=pdf

Singh, S., Young, A., & McNaught, C. E. (2017). The physiology of wound healing. *Surgery (United Kingdom)*. https://doi.org/10.1016/j.mpsur.2017.06.004

Sisson, K., Zhang, C., Farach-carson, M. C., Chase, D. B., & Rabolt, J. F. (2009). *Evaluation of Cross-Linking Methods for Electrospun Gelatin on Cell Growth and Viability*. *10*(7).

Song, Y. K., & Kim, C. K. (2006). Topical delivery of low-molecular-weight heparin with surface-charged flexible liposomes. *Biomaterials*, *27*(2), 271–280. https://doi.org/10.1016/j.biomaterials.2005.05.097

Sood, A., Granick, M. S., & Tomaselli, N. L. (2014). Wound Dressings and Comparative Effectiveness Data. *Advances in Wound Care*. https://doi.org/10.1089/wound.2012.0401

Staroszczyk, H., Sztuka, K., Wolska, J., Wojtasz-Pająk, A., & Kołodziejska, I. (2014). Interactions of fish gelatin and chitosan in uncrosslinked and crosslinked with EDC films: FT-IR study. *Spectrochimica Acta Part A: Molecular and Biomolecular Spectroscopy*, *117*, 707–712. https://doi.org/10.1016/J.SAA.2013.09.044

Sussman, C., & Bates-Jensen, B. (2012). wound care - A Collaborative Practice Manual for Health Professionals. In *Journal of Chemical Information and Modeling*. https://doi.org/10.1017/CBO9781107415324.004

Tanodekaew, S., Prasitsilp, M., Swasdison, S., Thavornyutikarn, B., Pothsree, T., & Pateepasen, R. (2004). Preparation of acrylic grafted chitin for wound dressing application. *Biomaterials*, *25*(7–8), 1453–1460. https://doi.org/10.1016/j.biomaterials.2003.08.020

Tansik, G., Yakar, A., & Gündüz, U. (2014). Tailoring magnetic PLGA nanoparticles suitable for doxorubicin delivery. *Journal of Nanoparticle Research*, *16*(1). https://doi.org/10.1007/s11051-013-2171-7

Templeton, D. M. (1988). The basis and applicability of the dimethylmethylene blue binding assay for sulfated glycosaminoglycans. *Connective Tissue Research*. https://doi.org/10.3109/03008208808992791

Tiwari, G., Tiwari, R., Sriwastawa, B., Bhati, L., Pandey, S., Pandey, P., & Bannerjee, S. K. (2012). Drug delivery systems: An updated review. *International Journal of Pharmaceutical Investigation*. https://doi.org/10.4103/2230-973X.96920

Tsala, D. E., Amadou, D., & Habtemariam, S. (2013). Natural wound healing and bioactive natural products. *Phytopharmacology*, *4*(3), 532–560.

Velnar, T., Bailey, T., & Smrkolj, V. (2009). The Wound Healing Process: an Overview of the Cellular and Molecular Mechanisms. In *The Journal of International Medical Research* (Vol. 37).

Viswanathan, P., Muralidaran, Y., & Ragavan, G. (2017). Challenges in oral drug delivery: A nano-based strategy to overcome. In *Nanostructures for Oral Medicine*. https://doi.org/10.1016/B978-0-323-47720-8.00008-0

Walters, K. A., & Roberts, M. S. (2002). *Dermatological and Transdermal Formulations - Google Kitaplar* (K. A. Walters, Ed.). Florida, US.

Wang, Y. J., & Zhag, Y. Q. (2011). Three-layered sericins around the silk fibroin fiber from Bombyx mori cocoon and their amino acid composition. *Advanced Materials Research*, *175–176*, 158–163. https://doi.org/10.4028/www.scientific.net/AMR.175-176.158

Wannatong, L., Sirivat, A., & Supaphol, P. (2004). Effects of solvents on electrospun polymeric fibers: Preliminary study on polystyrene. *Polymer International*, *53*(11), 1851–1859. https://doi.org/10.1002/pi.1599

Wei, Q., Tao, D., & Xu, Y. (2012). Nanofibers: Principles and manufacture. *Functional Nanofibers and Their Applications*, (1999), 3–21. https://doi.org/10.1016/B978-0-85709-069-0.50001-X

Yamashita, Y., Nakagomi, K., Takeda, T., Hasegawa, S., & Mitsui, Y. (1992). Effect of heparin on pulmonary fibroblasts and vascular cells. *Thorax*, *47*(8), 634–639. https://doi.org/10.1136/thx.47.8.634

Yang, G. Z., Li, H. P., Yang, J. H., Wan, J., & Yu, D. G. (2017). Influence of Working Temperature on The Formation of Electrospun Polymer Nanofibers. *Nanoscale Research Letters*, *12*(1). https://doi.org/10.1186/s11671-016-1824-8

Yang, W., Yang, F., Wang, Y., Both, S. K., & Jansen, J. A. (2013). In vivo bone generation via the endochondral pathway on three-dimensional electrospun fibers. *Acta Biomaterialia*, *9*(1), 4505–4512. https://doi.org/10.1016/j.actbio.2012.10.003

Zafar, M., Najeeb, S., Khurshid, Z., Vazirzadeh, M., Zohaib, S., Najeeb, B., & Sefat, F. (2016). Potential of electrospun nanofibers for biomedical and dental applications. *Materials*. https://doi.org/10.3390/ma9020073

Zahedi, P., Rezaeian, I., Ranaei-Siadat, S. O., Jafari, S. H., & Supaphol, P. (2010). A review on wound dressings with an emphasis on electrospun nanofibrous polymeric bandages. *Polymers for Advanced Technologies*. https://doi.org/10.1002/pat.1625

Zakharova, L., Pashirova, T., Kashapov, R., Gabdrakhmanov, D., & Sinyashin, O. (2017). Drug delivery mediated by confined nanosystems: structure-activity relations and factors responsible for the efficacy of formulations. In *Nanostructures for Drug Delivery*. https://doi.org/10.1016/b978-0-323-46143-6.00024-5

Zhang, Y. Z., Venugopal, J., Huang, Z. M., Lim, C. T., & Ramakrishna, S. (2006). Crosslinking of the electrospun gelatin nanofibers. *Polymer*. https://doi.org/10.1016/j.polymer.2006.02.046

Zhu, J., & Marchant, R. E. (2011). Design properties of hydrogel tissue-engineering scaffolds. *Expert Review of Medical Devices*. https://doi.org/10.1586/erd.11.27

APPENDICES

A. Calibration Curve of HP

Standard solutions of HP were used in distilled water to construct calibration curve by using DMMB assay (Figure A. 1). Linear calibration curve was obtained.

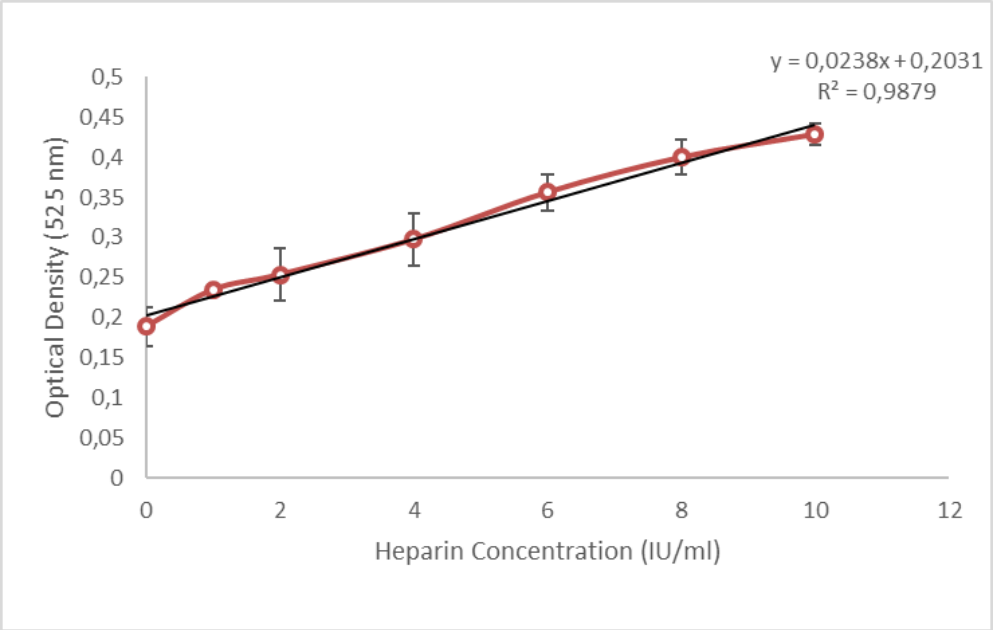

Figure A. 1. Calibration curve obtained from HP standards in distilled water with using DMMB assay. The data are represented as the mean ± Std. (n = 6).